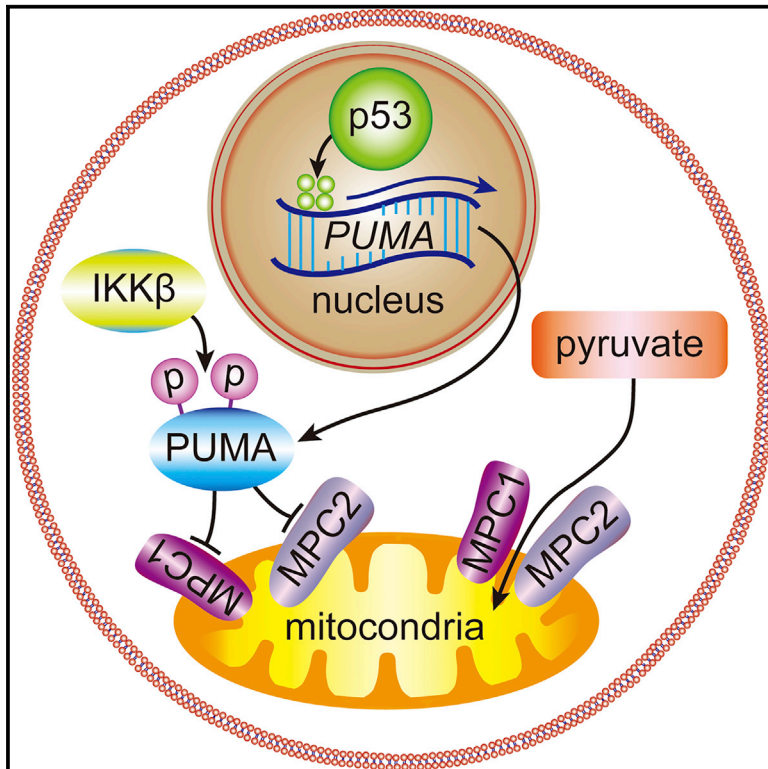


Cancer Cell

Wild-Type p53 Promotes Cancer Metabolic Switch by Inducing PUMA-Dependent Suppression of Oxidative Phosphorylation

Graphical Abstract



Authors

Jinchul Kim, Lili Yu,
Wancheng Chen, ..., Guihua Chen,
Xuemei Fu, Yang Xu

Correspondence

fxmzj2004@163.com (X.F.),
yangxu@ucsd.edu (Y.X.)

In Brief

Hepatocellular carcinomas (HCCs) often retain the wild-type p53. Kim et al. find that p53 is important for the growth of HCC cells and that p53-regulated PUMA reduces mitochondrial pyruvate uptake and increases glycolysis in HCC, suggesting caution when designing cancer treatment strategies that activate p53.

Highlights

- WTp53-PUMA pathway drives cancer metabolic switch
- PUMA suppresses mitochondrial pyruvate uptake by inactivating MPC
- IKKβ-mediated phosphorylation of PUMA is important for PUMA-MPC interaction
- High levels of PUMA in HCC are correlated with poor prognosis of HCC patients

Wild-Type p53 Promotes Cancer Metabolic Switch by Inducing PUMA-Dependent Suppression of Oxidative Phosphorylation

Jinchul Kim,^{1,2,3,4} Lili Yu,^{2,4} Wancheng Chen,² Yanxia Xu,² Meng Wu,² Dilyana Todorova,^{1,3} Qingshuang Tang,² Bingbing Feng,² Lei Jiang,² Jingjin He,¹ Guihua Chen,¹ Xuemei Fu,^{1,*} and Yang Xu^{1,2,3,5,*}

¹The Eighth Affiliated Hospital, Sun Yat-sen University, Shenzhen, Guangdong 518033, China

²Cancer Research Institute, Guangdong Provincial Key Laboratory of Cancer Immunotherapy, School of Basic Medical Sciences, Southern Medical University, Guangzhou, Guangdong 510515, China

³Division of Biological Sciences, University of California, San Diego, 9500 Gilman Drive, La Jolla, CA 92093-0322, USA

⁴These authors contributed equally

⁵Lead Contact

*Correspondence: fxmzj2004@163.com (X.F.), yangxu@ucsd.edu (Y.X.)

<https://doi.org/10.1016/j.ccell.2018.12.012>

SUMMARY

The tumor suppressor p53 is somatically mutated in half of all human cancers. Paradoxically, the wild-type p53 (Wtp53) is often retained in certain human cancers, such as hepatocarcinoma (HCC). We discovered a physiological and oncogenic role of Wtp53 in suppressing pyruvate-driven oxidative phosphorylation by inducing PUMA. PUMA inhibits mitochondrial pyruvate uptake by disrupting the oligomerization and function of mitochondrial pyruvate carrier (MPC) through PUMA-MPC interaction, which depends on I κ B kinase-mediated phosphorylation of PUMA at Ser96/106. High expression levels of PUMA are correlated with decreased mitochondrial pyruvate uptake and increased glycolysis in HCCs and poor prognosis of HCC patients. These findings are instrumental for cancer drug discovery aiming at activating Wtp53 or restoring Wtp53 activity to p53 mutants.

INTRODUCTION

It has been well established that p53 is critical to suppress cancer development in humans. As the “guardian of the genome,” p53 plays complex roles in cell-cycle arrest, apoptosis, and senescence, all of which likely contribute to the protection of the genome from accumulating mutations and passing these mutations to the daughter cells (Kasthuber and Lowe, 2017; Vousden and Prives, 2009). p53 also plays important roles in maintaining genomic stability of pluripotent stem cells by coordinating the DNA damage responses with pluripotency (Lin et al., 2005; Fu et al., 2017). As a transcription factor, p53 directly activates the transcription of a large panel of genes, including *CDKN1A*, *MDM2*, *PERP*, *PMAIP1*, *BBC3/PUMA*, and *CCNG1*

(Kruiswijk et al., 2015), and also directly suppresses the expression of a number of genes such as *MAP4* and *NANOG* (Lin et al., 2005; Murphy et al., 1996). These p53 target genes are required to mediate various p53-dependent functions in maintaining genomic stability. In response to various genotoxic and oncogenic stresses, p53 is rapidly stabilized and activated via translational and posttranslational mechanisms (Meek, 2015; Xu, 2003). The interaction between p53 and E3 ligases such as MDM2, the gene encoding which is a transcriptional target of p53, leads to rapid degradation of p53 in normal cells (Wade et al., 2013). The interaction between p53 and MDM2 or MDM4 also suppresses the transcriptional activities of p53. The stress-induced phosphorylation of p53 at its N terminus can disrupt the interaction between p53 and MDM2/MDM4,

Significance

Glycolysis is a hallmark of cancer metabolism and is required for tumorigenesis. In contrast to the current paradigm in which Wtp53 plays multiple roles in promoting oxidative phosphorylation and inhibiting glycolysis by regulating the expression or activity of metabolic enzymes, we discovered a dominant metabolic role of Wtp53 in promoting cancer metabolic switch from oxidative phosphorylation to glycolysis by inducing PUMA-mediated disruption of mitochondrial pyruvate uptake. This role of Wtp53 can resolve several long-lasting paradoxes in p53 biology and will be instrumental in the development of cancer therapy, especially in the context of the highly pursued strategies to eliminate human cancer by either activating Wtp53 or restoring Wtp53 function to p53 mutants in cancers.

leading to p53 activation (Chao et al., 2000, 2006; Craig et al., 1999; Liu et al., 2010; Saito et al., 2003; Shieh et al., 2000).

Despite intensive studies, the roles of p53 in tumor suppression remain unclear (Mello and Attardi, 2018). p53-dependent cell-cycle arrest alone is not required for p53-dependent tumor suppression (Brugarolas et al., 1995; Deng et al., 1995). p53-dependent apoptosis appears to be dispensable for p53-dependent tumor suppression, because PUMA-deficient mice, in which p53-dependent apoptosis is abolished, are not cancer prone (Jeffers et al., 2003; Villunger et al., 2003). In contrast, PUMA is overexpressed in many human cancers (Cai et al., 2013; Du et al., 2012; Kim et al., 2007) and the loss of PUMA ablates tumorigenesis in certain mouse models (Michalak et al., 2010; Qiu et al., 2011), suggesting that PUMA could function as an oncogene. In addition, p53 R172P mutant knockin mice, which are completely defective in p53-dependent apoptosis, are not prone to cancer (Liu et al., 2004). Knockin mice defective in p53-dependent cell-cycle arrest, apoptosis, and senescence do not have increased frequency of spontaneous tumorigenesis (Jiang et al., 2011; Li et al., 2012).

Considering the critical roles of glycolysis in tumorigenesis (Hanahan and Weinberg, 2011), accumulating data support the notion that p53 might confer tumor suppression by inhibiting glycolysis and promoting oxidative phosphorylation (Shen et al., 2012). In this context, numerous reports have shown that p53 exerts this metabolic regulation by regulating the expression of metabolic genes, such as p53-induced glycolysis and apoptosis regulator (*TIGAR*) and glucose transporters; synthesis of cytochrome c oxidase 2, glutaminase 2, and malic enzyme; or protein-protein interactions with metabolic enzymes, such as glucose-6-phosphate dehydrogenase, peroxisome-proliferator-activated receptor γ coactivator-1, and SREBP (Humpton and Vousden, 2016; Kruiswijk et al., 2015). These data support the current paradigm in which wild-type p53 (Wtp53) suppresses tumorigenesis by inhibiting cancer metabolic switch from oxidative phosphorylation to glycolysis (Kruiswijk et al., 2015).

Consistent with the notion that the inactivation of Wtp53 is required for cancer initiation and development, genomic DNA sequencing of human cancers indicates that the p53 gene (*TP53*) is somatically mutated in over 50% of all human cancers (Bykov et al., 2017). In addition to the loss of Wtp53 activity, the expressed p53 mutants gain oncogenic activities to promote drug resistance, glycolysis, and other aspects of tumorigenesis (Bykov et al., 2017; Xu, 2008). The inactivation of p53 activity can be achieved through multiple mechanisms, including overexpression of the p53 inhibitor MDM2/MDM4 or disruption of pathways required for Wtp53 activation (Bykov et al., 2017). However, the frequency of p53 mutation remains low in certain types of human cancers such as hepatocellular carcinoma (HCC) (Soussi and Wiman, 2007). Considering that genetic instability is a hallmark of human cancers, and cancer cells are under intensive selection for pro-survival genetic mutations (Hanahan and Weinberg, 2011), it remains a paradox why the somatic mutation of *TP53* is not selected for in these cancers. Therefore, in contrast to the general assumption that Wtp53 functions as a tumor suppressor, we hypothesize that Wtp53 might play oncogenic roles in promoting tumorigenesis of human cancers harboring Wtp53.

RESULTS

Wtp53 Is Required for Tumorigenesis of HCC Cells

To examine the roles of Wtp53 in human cancer cells, we silenced the expression of Wtp53 in human cancer cells with the tetracycline-inducible p53 short hairpin RNA (shRNA) system. The knockdown (KD) of Wtp53 was achieved after doxycycline (Doxy, 1 μ g/mL) treatment for 4 days, leading to the downregulation of the p53 target gene *PUMA* in some human cancer cells (Figures S1A and S1B). In contrast to the general assumption that Wtp53 suppresses tumorigenesis, the KD of p53 inhibited the proliferation of four HCC cell lines harboring Wtp53 (HepG2, SK-Hep1, BEL7404, and SMAC7721 cells) but had no apparent impact on other human cancer cell lines harboring Wtp53 (Figure 1A). Considering the importance of glycolysis in cancer cell proliferation (Hanahan and Weinberg, 2011), to understand the basis of the differential impact of Wtp53 KD on the proliferation of various human cancer cell lines, we analyzed the impact of Wtp53 KD on glycolysis. The KD of Wtp53 decreased glycolysis in the four HCC cell lines but not other human cancer cell lines, supporting the notion that the impaired proliferation was due to the inhibition of glycolysis in these HCC cells after p53 depletion (Figures 1B and 1C). Consistent data were obtained using distinct p53 shRNAs, ruling out the possibility of off-target effects (Figures S2A–S2C). To further understand how Wtp53 promotes glycolysis in these HCC cells, we analyzed the pyruvate-driven oxidative phosphorylation (OXPHOS) activity in these cells. Our data indicated that p53 KD significantly increased pyruvate-driven ATP production in HCC cells but not in other human cancer cell lines, suggesting that Wtp53 suppresses mitochondrial OXPHOS in these HCC cells (Figure 1D).

Because *TP53* is not frequently mutated in HCC (Soussi and Wiman, 2007), we focused on two HCC cell lines (HepG2 and SK-Hep1) to further investigate the roles of Wtp53 in tumorigenesis. Wtp53 can be activated by RITA, a small-molecule p53 activator (Issaeva et al., 2004). Treatment of HepG2 cells with RITA (0.3 μ M) modestly increased the expression of p53 target genes such as *PUMA* and *CDKN1A*, and promoted glycolysis in a p53-dependent manner (Figures 1E–1G). This dosage of RITA did not induce apoptosis of HCC cells (Figure S2D). The activation of Wtp53 in SK-Hep1 cells by RITA also induced the expression of *PUMA* and *CDKN1A* as well as glycolysis (Figures S2E and S2F). Therefore, the modest activation of Wtp53 in HCCs promotes cancer metabolic switch without inducing significant apoptosis.

Consistent with the findings that the KD of Wtp53 inhibited the cellular proliferation and glycolysis of HepG2 and SK-Hep1 cells but not those of HeLa and HCT116 cells, the KD of Wtp53 greatly suppressed the *in vivo* tumorigenesis of HepG2 and SK-Hep1 cells but not that of HeLa and HCT116 cells (Figures 1H, 1I, and S2G–S2I). These data supported the notion that Wtp53 is required for the tumorigenesis and glycolytic metabolism of HCC cells. Human cancer cells such as HeLa and HCT116 cells derived their energy primarily from glycolysis, and their OXPHOS activity had essentially been abolished via Wtp53-independent mechanisms (Figures 1B, 1C, and S2I). In summary, these findings suggest that Wtp53 is required to maintain cancer metabolic switch in human cancer cells with relatively higher mitochondrial OXPHOS activity.

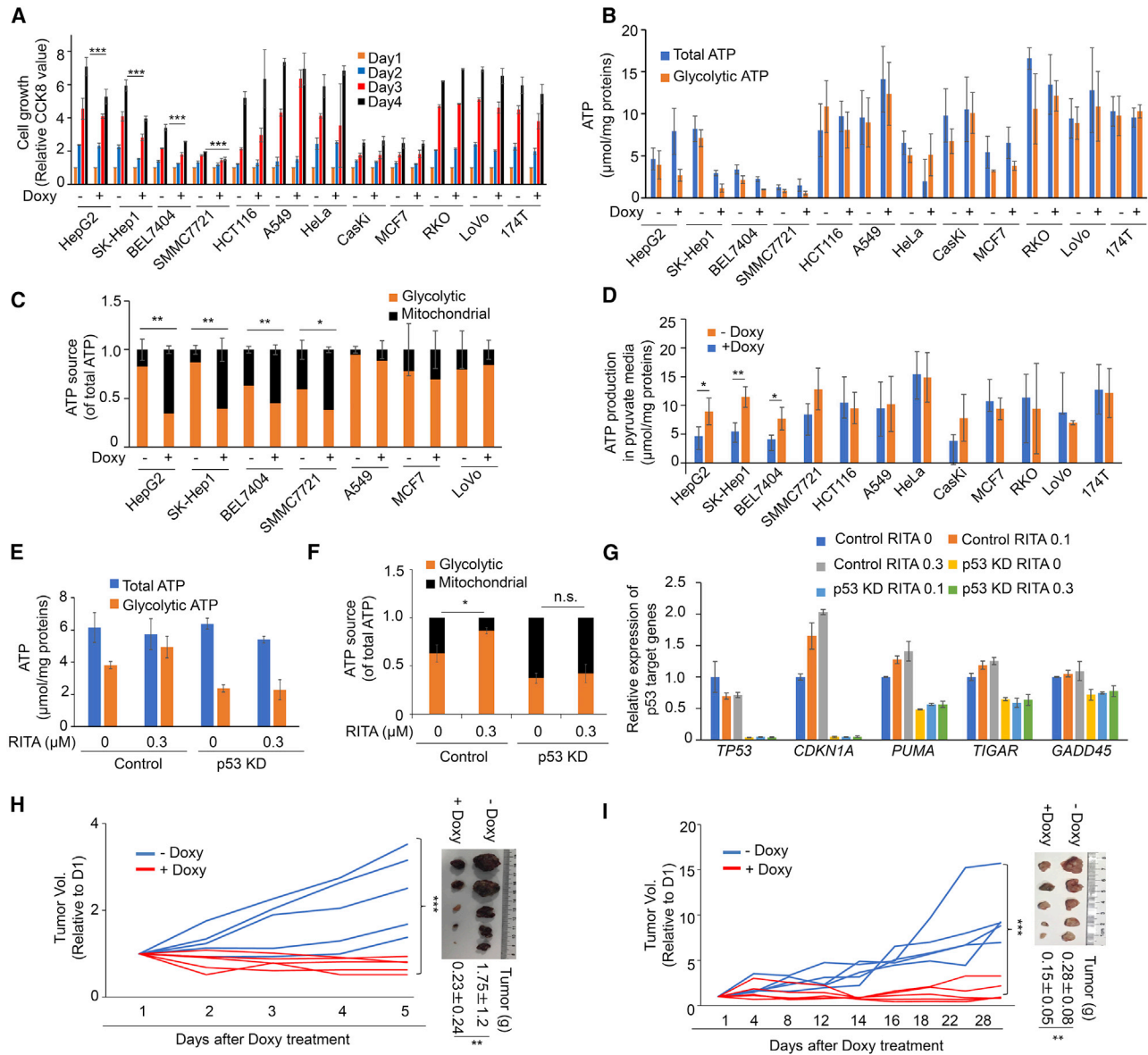


Figure 1. WTp53 Is Required to Maintain Growth and Glycolysis of Some Human Cancer Cells

(A) The proliferation of 12 human cancer cell lines after the inducible knockdown (KD) of WTp53 achieved by the transduction of lentivirus harboring tetracycline-inducible p53 shRNA. $n = 3$. Data are represented as mean \pm SD. Repeated-measures ANOVA, followed by Bonferroni post-tests.

(B) Levels of total ATP and glycolytic ATP of 12 human cancer cell lines before and after p53 KD. $n = 3$. Data are represented as mean \pm SD.

(C) The proportion of glycolytic ATP and mitochondrial ATP (total ATP – glycolytic ATP) of seven lines of cancer cells before and after p53 KD. Unpaired t test. $n = 3$. Data are represented as mean \pm SD.

(D) Total ATP measurement of the cancer cells before and after p53 KD. Cancer cells were cultured for 8 h in DMEM containing pyruvate as the only mitochondrial energy source (10 mM). $n = 4$. Data are represented as mean \pm SD.

(E and F) The glycolytic ATP production (E) and mitochondrial ATP production (F) in control and p53 KD HepG2 cells after RITA (0.3 μ M) treatment for 24 h. $n = 3$. Data are represented as mean \pm SD.

(G) The expression of various p53 target genes in HepG2 cells after RITA (0.3 μ M) treatment for 24 h. $n = 3$. Data are represented as mean \pm SD.

(H and I) Individual tumor volume of tumors formed by HepG2 (H) or SK-Hep1 (I) cells without or with inducible KD of WTp53 in immunodeficient NSG mice measured every day after Doxy treatment and compared with the volume of day 1 (left). Repeated-measures ANOVA, followed by Bonferroni post-tests. $n = 5$ (each group). At the end of the Doxy treatment, all tumors were weighed and photographed (right). $n = 5$ (each group).

Data are represented as mean \pm SD. * $p < 0.05$, ** $p < 0.01$, and *** $p < 0.001$ denote significant differences. n.s. denotes non-significant. See also [Figures S1](#) and [S2](#).

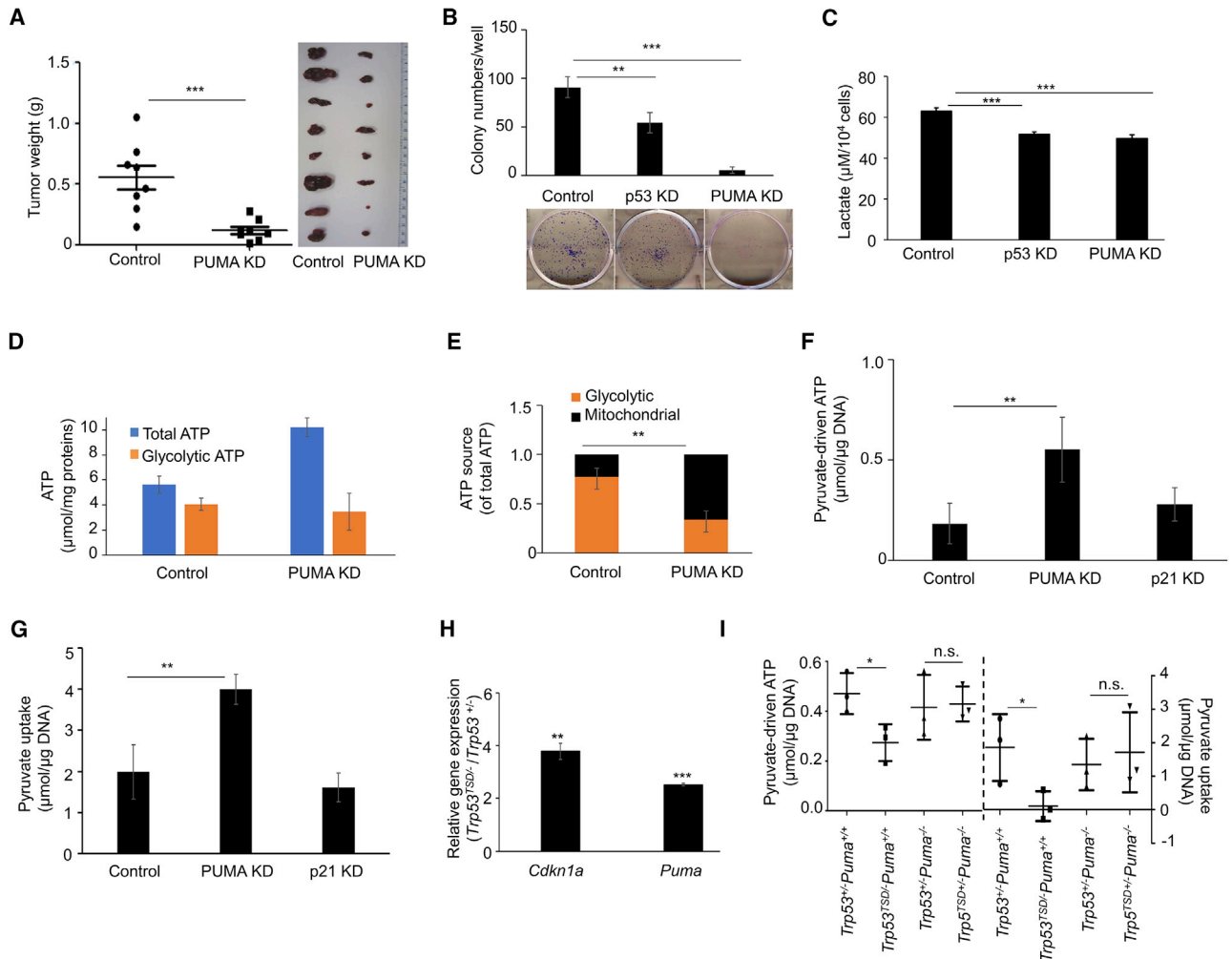


Figure 2. PUMA Mediates the WTP53-Dependent Cancer Metabolic Switch in HCC Cells

(A) Quantification of tumor weight (left) and photographs (right) of tumors recovered 5 weeks after implantation of control and PUMA KD HepG2 cells. Mann Whitney test. $n = 8$. Data are represented as mean \pm SD.

(B) Representative images of colonies revealed by crystal violet staining and quantification of colony numbers of control, p53 KD, and PUMA KD HepG2 cells. One-way ANOVA, followed by Dunnett's multiple comparison test. $n = 3$. Data are represented as mean \pm SD.

(C) Lactate production of control, p53 KD, and PUMA KD HepG2 cells. One-way ANOVA, followed by Dunnett's multiple comparison test. $n = 3$. Data are represented as mean \pm SD.

(D and E) Glycolytic ATP production (D) and mitochondrial ATP production (E) in control and PUMA KD HepG2 cells. Unpaired t test. $n = 3$. Data are represented as mean \pm SD.

(F) ATP production from mitochondria isolated from control, PUMA KD, and p21 KD HepG2 cells in the presence of 1 mM ADP and the respiration substrates 5 mM pyruvate and 5 mM malate. One-way ANOVA, followed by Dunnett's multiple comparison test. $n = 4$. Data are represented as mean \pm SD.

(G) Pyruvate uptake into mitochondria in control, PUMA KD, and p21 KD HepG2 cells. One-way ANOVA, followed by Dunnett's multiple comparison test. $n = 4$. Data are represented as mean \pm SD.

(H) mRNA levels of *Cdkn1a* and *Puma* in the liver of *Trp53^{TSD/+}* mice compared with that in *Trp53^{+/-}* mice. Paired t test. $n = 3$. Data are represented as mean \pm SD.

(I) Pyruvate-driven ATP production (left y axis) and mitochondrial pyruvate uptake (right y axis) in mitochondria isolated from the livers of *Trp53^{TSD/-}* mice, *Trp53^{+/-}* mice, *Trp53^{+/-} Puma^{-/-}* mice, and *Trp53^{TSD/-} Puma^{-/-}* mice. $n = 3$ for each genotype of mice.

Data are represented as mean \pm SD. Unpaired t test. * $p < 0.05$, ** $p < 0.01$, and *** $p < 0.001$ denote significant difference. n.s. denotes non-significant. See also Figure S3.

PUMA Mediates WTP53-Dependent Suppression of OXPHOS in HCC Cells

To understand the mechanism of how WTP53 suppresses mitochondrial OXPHOS, we focused on PUMA, which is a transcriptional target of p53 and encodes a mitochondrial protein required for p53-dependent apoptosis (Jeffers et al., 2003; Villunger et al.,

2003). In addition, experimental and clinical data suggest that PUMA is oncogenic (Hikisz and Kiliańska, 2012). PUMA KD in HepG2 cells greatly inhibited their growth *in vitro* and *in vivo*, supporting the notion that PUMA mediates WTP53 function in promoting tumorigenesis of HCC cells (Figures 2A and 2B). In addition, similar to the impact of WTP53 KD on OXPHOS of

HepG2 cells, PUMA KD in HepG2 cells inhibited the production of glycolytic ATP and lactate (Figures 2C–2E). PUMA KD, but not p21 KD, increased the pyruvate-driven OXPHOS and pyruvate mitochondrial uptake (Figures 2F and 2G). By generating PUMA knockout (PUMA KO) HepG2 cells using the CRISPR/CAS9 approach (Figures S3A–S3C), we showed that PUMA was important for Wtp53-dependent suppression of OXPHOS in HepG2 cells after RITA treatment (Figure S3D). Because the inhibition of mitochondrial pyruvate uptake inhibits OXPHOS and induces glycolysis (Schell et al., 2014), these data indicate that PUMA mediates the roles of Wtp53 in promoting metabolic switch from OXPHOS to glycolysis in some HCC cells. The silencing of PUMA appears to have a more dramatic impact on OXPHOS than silencing of Wtp53, suggesting that Wtp53 is only one of the inducers of PUMA in human cancer cells.

To confirm the physiological relevance of this metabolic role of the p53-PUMA axis, we examined the roles of p53 and PUMA in mitochondrial pyruvate metabolism in mouse liver. Using the *Trp53*^{TSD} (Thr18Ser20 mutated to Asp) knockin mouse model with constitutively active p53 (Liu et al., 2010) and *Puma*^{-/-} mice (Jeffers et al., 2003), we showed that the activation of p53 in mouse liver increased the expression of *Puma* and *Cdkn1a* (Figure 2H). In addition, Wtp53 suppressed mitochondrial pyruvate uptake and pyruvate-driven mitochondrial ATP production in mouse hepatocytes in a PUMA-dependent manner (Figure 2I). Therefore, the p53-PUMA pathway plays an evolutionarily conserved and physiological role in inhibiting mitochondrial pyruvate uptake and OXPHOS.

PUMA Inhibits Mitochondrial Pyruvate Uptake by Disrupting the Function of MPC

Mitochondrial pyruvate carrier (MPC), a mitochondrial membrane complex composed of MPC1 and MPC2 proteins, is important to transport pyruvate into mitochondria (Herzig et al., 2012). To elucidate the mechanism of how PUMA inhibits mitochondrial pyruvate uptake, we hypothesized that PUMA, also a mitochondrial membrane protein (Wilfling et al., 2012), might inhibit the function of MPC through protein-protein interaction. Using co-immunoprecipitation (CO-IP), we demonstrated that the overexpressed PUMA isoforms α and β interacted with MPC (Figure 3A). Consistent with this finding, the interaction between the endogenous MPC and PUMA was confirmed in HepG2 cells with CO-IP (Figure 3B). To further validate the interaction between MPC and PUMA in live cells, we employed fluorescence resonance energy transfer (FRET) assay in live cells co-expressing eGFP-tagged MPC2 and mCherry-tagged PUMA or various deletion mutants of PUMA. The data demonstrated that the full-length PUMA and two PUMA deletion mutants (del92 and delBH3) interacted with MPC2 in live cells, but PUMA deletion mutant (del137) failed to interact with MPC2, indicating that the PUMA domain between amino acids (aa) 92 and 137 is required for the interaction with MPC2 (Figure 3C). To examine the interaction between endogenous PUMA and MPC in HepG2 cells, we used confocal immunofluorescence analysis to show close colocalization of the endogenous PUMA and MPC1 in HepG2 cells (Figure S4A). In addition, using primary antibodies against PUMA and MPC1 followed by Cy5/Cy3 conjugated secondary antibodies, we showed significant FRET efficiency (>10%) between endogenous PUMA and

MPC1, indicating significant interaction between the endogenous PUMA and MPC1 (Figures S4B and S4C).

Since the oligomerization of MPC1 and MPC2 is required for the function of MPC to transport pyruvate into mitochondria (Herzig et al., 2012), we examined the impact of PUMA on the oligomerization of MPC1 and MPC2. PUMA KO in HepG2 cells increased the hetero-oligomerization of MPC1 and MPC2 as well as the homo-oligomerization of MPC2 (Figure 3D). In support of this conclusion, using FRET assay, we demonstrated that PUMA inhibited both the homo-oligomerization of MPC2 and the hetero-oligomerization of MPC1 and MPC2 in live 293 cells (Figure 3E). As predicted from the PUMA-MPC2 interaction data, when ectopically expressed in PUMA KO cells at the endogenous levels that did not induce apoptosis, both PUMA and PUMA mutant (delBH3) effectively suppressed MPC-dependent pyruvate uptake into the mitochondria and rescued the proliferation defects of PUMA KO cells (Figures S4D–S4G). Therefore, PUMA inhibits the mitochondrial pyruvate uptake by disrupting the oligomerization and function of the MPC complex.

IKK β -Mediated Phosphorylation of PUMA Is Required for PUMA Interaction with MPC

To further understand the mechanism regulating the interaction between PUMA and MPC, we focused on the central domain (aa 92–137) of PUMA that is required for the interaction between MPC and PUMA. There are three potential phosphorylation sites at Ser10, Ser96, and Ser106 of PUMA (Fricker et al., 2010), two of which are located within the region of PUMA required for its interaction with MPC. Using the phosphorylation site prediction software GPS (3.538 score in high threshold cutoff) (Xue et al., 2005), we predicted that S96 and S106 could be the phosphorylation sites of I κ B kinase β (IKK β). In support of this notion, we showed that the inhibition of IKK β kinase activity with specific inhibitors prevented the Ser/Thr phosphorylation of PUMA after tumor necrosis factor alpha (TNF- α) stimulation (Figure 4A). In addition, the IKK β -mediated phosphorylation of the phosphorylation site mutant (S96/106A) of PUMA, denoted MT PUMA, was significantly reduced compared with that of WT PUMA after TNF- α stimulation (Figure 4B). Together, these data indicate that IKK β phosphorylates PUMA at S96 and S106. While it has been reported that the phosphorylation of PUMA at S10 regulates its apoptotic function (Fricker et al., 2010), the phosphorylation of PUMA at S96 and S106 did not affect its protein stability and apoptotic activity (Figures S5A–S5D).

To elucidate the roles of IKK β in PUMA-MPC interaction, we examined the impact of the increased IKK β expression on the oligomerization of MPC1 and MPC2. The increased expression of IKK β promoted the interaction between PUMA and MPC and decreased the oligomerization of MPC1 and MPC2, suggesting that phosphorylation of PUMA at S96/106 by IKK β promotes the interaction between PUMA and MPC (Figure 4C). The IKK β pathway is oncogenic and drives the cancer metabolic switch from OXPHOS to glycolysis in human cancer cells (Tornatore et al., 2012). To test the involvement of the PUMA-MPC pathway in the metabolic roles of IKK β , we examined the importance of PUMA in IKK β -driven mitochondrial pyruvate uptake and found that the overexpression of IKK β suppressed mitochondrial pyruvate uptake in a PUMA-dependent manner (Figure 4D). These data support the hypothesis that the

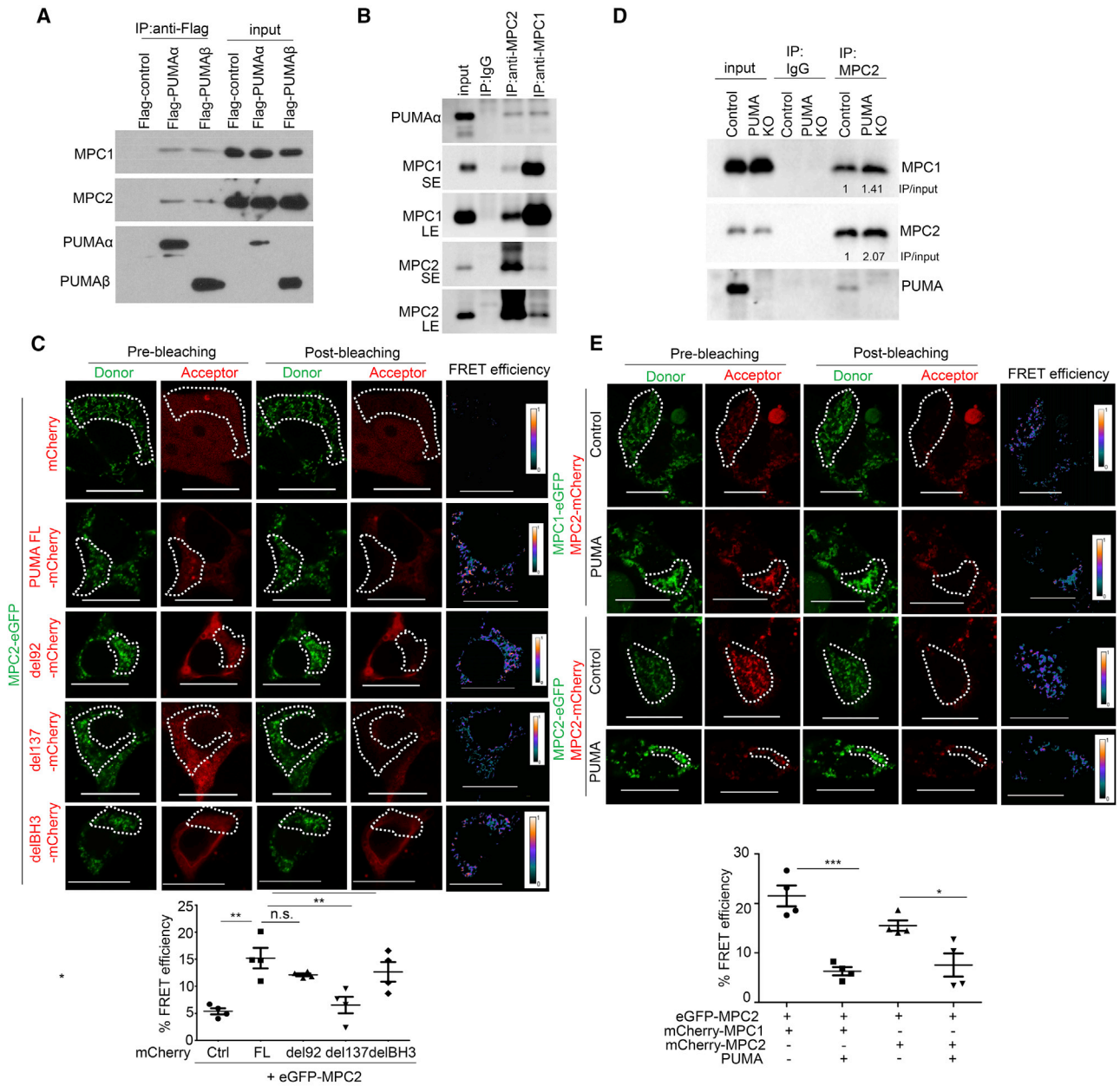


Figure 3. PUMA Interacts with MPC and Inhibits the Oligomerization of MPC1 and MPC2

(A) Mitochondrial fraction of 293T cells transfected with indicated expression vectors was subjected to immunoprecipitation (IP) with anti-FLAG antibody. The presence of MPC1 and MPC2 in the immunoprecipitate was examined by western blotting.

(B) Mitochondrial fraction of HepG2 cells was subjected to IP with anti-MPC1 or anti-MPC2 antibody. The presence of PUMA in the immunoprecipitate was examined by western blotting. Both short exposure (SE) and long exposure (LE) are shown.

(C) FRET analysis was performed in 293T cells overexpressing MPC2-eGFP and PUMA-mCherry or the deletion mutants of PUMA. The deletion mutants of PUMA included deletion of the first 92 aa (del92), the first 137 aa (del137), and the BH3 domain (delBH3) of PUMA. Donor and acceptor images were collected before and after bleaching (top), and FRET efficiency was calculated and presented (bottom). One-way ANOVA, followed by Bonferroni's multiple comparison test. $n = 4$. Data are represented as mean \pm SD. Scale bars, 20 μ m.

(D) Mitochondrial fractions of PUMA wild-type (WT) and PUMA KO HepG2 cells were immunoprecipitated with anti-MPC2 antibody followed by western blotting analysis for MPC1 and MPC2.

(E) FRET analysis was performed in 293T cells overexpressing MPC2-mCherry with either MPC1-eGFP or MPC2-eGFP with or without PUMA overexpression. Donor and acceptor images were collected before and after bleaching (top), and FRET efficiency was calculated and presented (bottom). Unpaired t test. $n = 4$. Data are represented as mean \pm SD. Unpaired t test. * $p < 0.05$, ** $p < 0.01$, and *** $p < 0.001$ denote significant difference. n.s. denotes non-significant. Scale bars, 20 μ m. See also Figure S4.

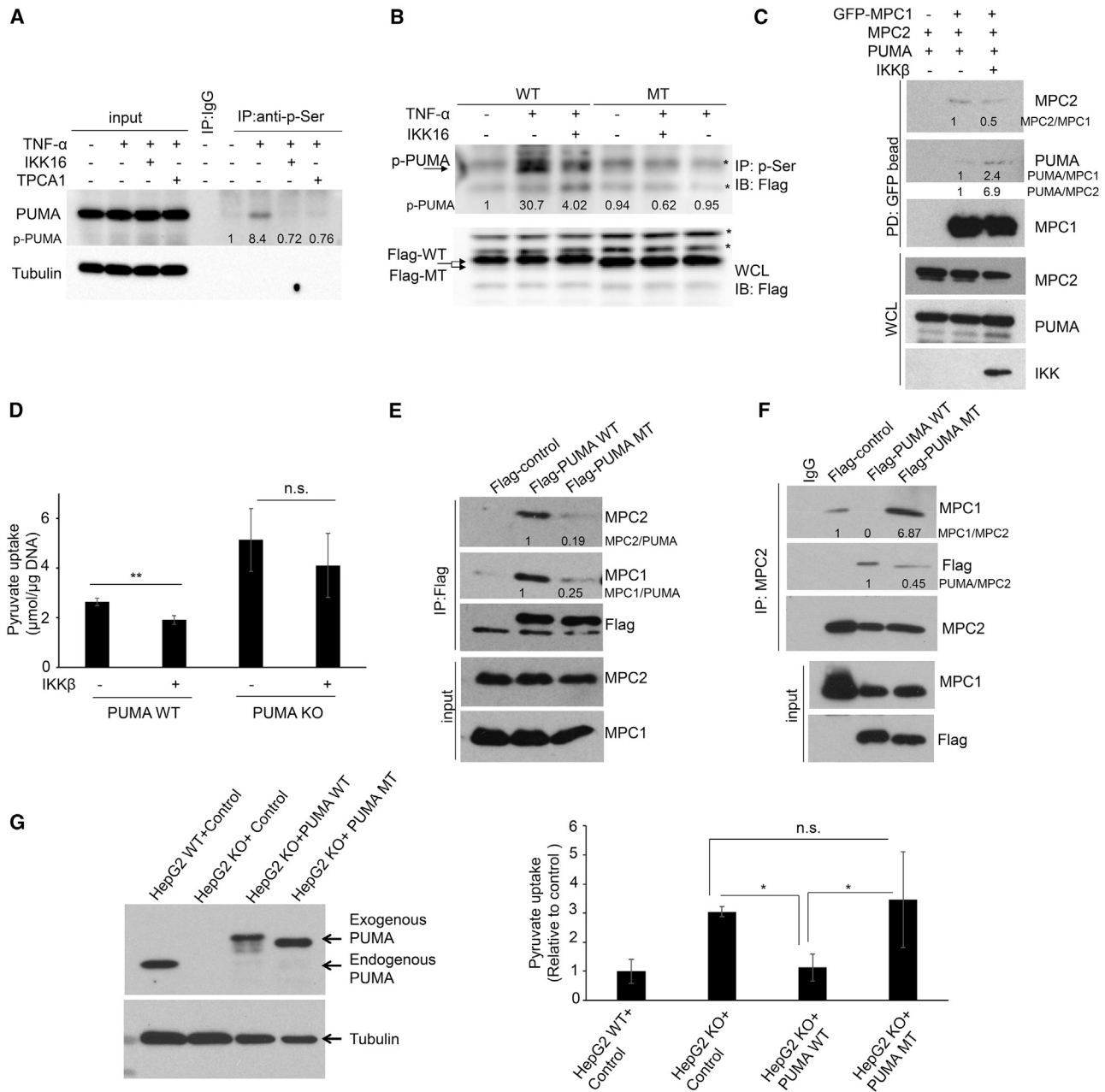


Figure 4. IKK β -Mediated Phosphorylation of PUMA at S96/106 Is Important for PUMA-MPC Interaction

(A) IKK β in HepG2 cells was activated by TNF- α (50 ng/mL) for 2 h and then treated with IKK β -specific inhibitors (IKK16 and TPCA-1, 5 μM). Cell lysates were subjected to IP with an antibody specific for phosphorylated serine (anti-p-Ser). The presence of PUMA in the resulting precipitate was detected with anti-PUMA antibody.

(B) HepG2 cells were transduced by lentivirus harboring tetracycline-inducible vectors expressing WT PUMA-FLAG or MT PUMA (S96/106A)-FLAG. Cells were incubated in serum-free medium for 24 h before being treated with IKK16 (5 μM) for 2 h, followed by TNF- α stimulus (50 ng/mL) for 2 h. Cell lysates were subjected to IP with antibody specific for phosphorylated serine. The presence of PUMA in the resulting precipitate was detected by anti-FLAG antibody. Asterisk (*) indicates non-specific band.

(C) 293T cells transfected with the indicated expression vectors were subjected to pull-down with magnetic anti-GFP beads, and the resulting precipitates were subjected to western blotting analysis with antibodies specific for MPC1, MPC2, PUMA, and IKK β .

(D) PUMA WT or PUMA KO HepG2 cells were transfected with IKK β expression vector or empty expression vectors. Mitochondria were isolated to measure MPC-dependent mitochondrial pyruvate uptake. Unpaired t test. n = 3. Data are represented as mean \pm SD. **p < 0.01 and n.s., non-significant.

(E) 293T cells were transfected with indicated expression vectors and cell lysates subjected to IP with anti-MPC2 antibody. The resulting precipitates were subjected to western blotting analysis with antibodies specific for MPC1, MPC2, and FLAG-PUMA.

(F) Cell lysates of 293T cells transfected with indicated expression vectors were subjected to IP with anti-FLAG antibody. The resulting precipitates were subjected to western blotting analysis with antibodies specific for MPC1, MPC2, and FLAG-PUMA.

(legend continued on next page)

phosphorylation of PUMA at Ser96/106 by IKK β promotes the interaction between PUMA and MPC, leading to the suppression of mitochondrial pyruvate uptake.

To further test this hypothesis, we compared the impact of the overexpression of WT PUMA and MT PUMA on the PUMA-MPC interaction. In contrast to WT PUMA, MT PUMA could neither efficiently interact with the MPC complex (Figure 4E) nor disrupt the oligomerization of MPC1/2 (Figure 4F). In addition, the restored expression of WT PUMA but not MT PUMA in PUMA KO HepG2 cells could suppress MPC-dependent mitochondrial pyruvate uptake (Figure 4G). In this context, the phosphorylation of PUMA at S96/S106 appeared to promote the recruitment of PUMA from cytoplasm to mitochondria (Figure S5E). These data indicate that IKK β -mediated phosphorylation of PUMA at S96/106 is important for PUMA-mediated inhibition of mitochondrial pyruvate uptake. Therefore, PUMA represents a novel functional link to confer the synergy of the oncogenic roles of WTP53 and IKK β in promoting cancer metabolic switch.

High Levels of PUMA in HCC Are Positively Correlated to Reduced Mitochondrial Pyruvate Uptake and Increased Glycolysis

To investigate the clinical relevance of PUMA-dependent metabolic functions in the tumorigenesis of HCC, we examined the levels of PUMA, lactate, and pyruvate in freshly resected HCC samples from patients. Consistent with the conclusion that PUMA promotes the metabolic switch from OXPHOS to glycolysis, high protein levels of PUMA were modestly correlated to higher levels of lactate and cytoplasmic pyruvate in HCC samples (Figures 5A–5C). To determine the correlation of PUMA levels and mitochondrial pyruvate uptake in HCCs, the mitochondria were isolated from HCCs and examined for mitochondrial pyruvate uptake. We treated the mitochondria with the MPC inhibitor UK5099 and divided the samples into two groups based on mitochondrial pyruvate uptake levels (Figure 5D). The levels of PUMA and lactate in HCCs were inversely correlated with the levels of mitochondrial pyruvate uptake (Figures 5E and 5F). In summary, these data indicate the clinic relevance of PUMA-dependent metabolic roles in HCCs by inhibiting mitochondrial pyruvate uptake and OXPHOS.

High Levels of PUMA in HCC Are Correlated with the Poor Prognosis of the HCC Patients

Since PUMA promotes the cancer metabolic switch that favors tumorigenesis, we hypothesized that the levels of PUMA in HCC can predict the clinical outcome of HCC patients. To test this hypothesis, we analyzed the mRNA levels of *PUMA* in a cohort of HCC cases. Compared with those of the matched adjacent normal tissue, the mRNA levels of *PUMA* but not *CDKN1A* were significantly higher in HCC (Figures 6A–6D). Based on the mRNA levels of *PUMA* in HCC, a cohort of HCC patients with 3 years of recurrence-free survival (RFS) or less were divided into two groups: patients with high *PUMA* expression

in HCCs (top 25%) and the rest of the patients. Patients with high *PUMA* expression in HCC exhibited significantly shorter RFS than the patients having lower *PUMA* expression in HCC ($p = 0.0116$), but the mRNA levels of *CDKN1A* had no correlation with the RFS of HCC patients ($p = 0.4528$) (Figures 6E and 6F), even when those having HCC with mutant *TP53* were removed from the analysis (Figure 6G). To further determine the prognostic value of *PUMA* expression levels in some common clinicopathological parameters associated with RFS of HCC patients, univariate and multivariate analyses were performed. The univariate analysis showed that *PUMA* expression levels were significantly associated with three-pathological markers such as tumor number, microvascular invasion (MVI), and portal vein tumor thrombosis (PVTT) (Table 1). Multivariate Cox proportional hazards model indicated that the expression levels of *PUMA* were an independent prognostic marker for RFS of HCC patients, after adjustment for tumor number, MVI, and PVTT. In summary, high levels of PUMA expression in HCC are correlated with poor prognosis of HCC patients.

DISCUSSION

WTP53 plays multiple roles in promoting OXPHOS and inhibiting glycolysis by regulating the expression or activity of metabolic enzymes, and thus contributing to the tumor suppression activity of p53 by disrupting cancer metabolism (Kruiswijk et al., 2015). In contrast to this paradigm, we discovered an oncogenic role of WTP53 in promoting the cancer metabolic switch by dominantly suppressing OXPHOS. The physiological relevance of this discovery is further supported by our findings that WTP53 plays the same role in mouse liver. This metabolic role of p53 also explains previous findings that the acute depletion of p53 in mouse liver and fibroblasts leads to enhanced OXPHOS (Prokesch et al., 2016; Lake et al., 2012). By suppressing the mitochondrial uptake of pyruvate, the key substrate for OXPHOS, this metabolic role of p53 can overcome other roles of p53 in promoting OXPHOS in glucose metabolism, leading to a net decrease in OXPHOS and an increase in glycolysis. For example, the p53-dependent induction of AIF and SCO2 cannot increase the OXPHOS activity in the absence of substrate pyruvate in the mitochondria.

Our conclusion can also explain some unresolved puzzles in p53 biology. For example, considering that adult stem cells primarily rely on glycolysis for energy and maintenance, our conclusion could explain the paradoxical findings that mice with modestly increased p53 activities exhibit increased resistance to tumorigenesis but normal or even longer life span than WT mice (Garcia-Cao et al., 2002; Matheu et al., 2007; Mendrysa et al., 2006). Because OXPHOS is the primary source of oxidative stress that induces genomic DNA damage, the p53-dependent suppression of OXPHOS will contribute to p53-dependent maintenance of genomic stability in normal cells with high OXPHOS activity, such as liver cells. In addition, this metabolic role of

(G) PUMA KO HepG2 cells were transduced with lentivirus harboring an inducible expression cassette of WT PUMA (WT) or phosphorylation sites mutant PUMA (MT) or empty expression vector. The expression levels of WT and MT PUMA in PUMA KO cells after 8 h of Doxy treatment are shown (left). Mitochondria were isolated to measure the MPC-dependent mitochondrial pyruvate uptake (right). $n = 3$. Data are represented as mean \pm SD. One-way ANOVA, followed by Bonferroni's multiple comparison test. * $p < 0.05$ and n.s., non-significant. See also Figure S5.

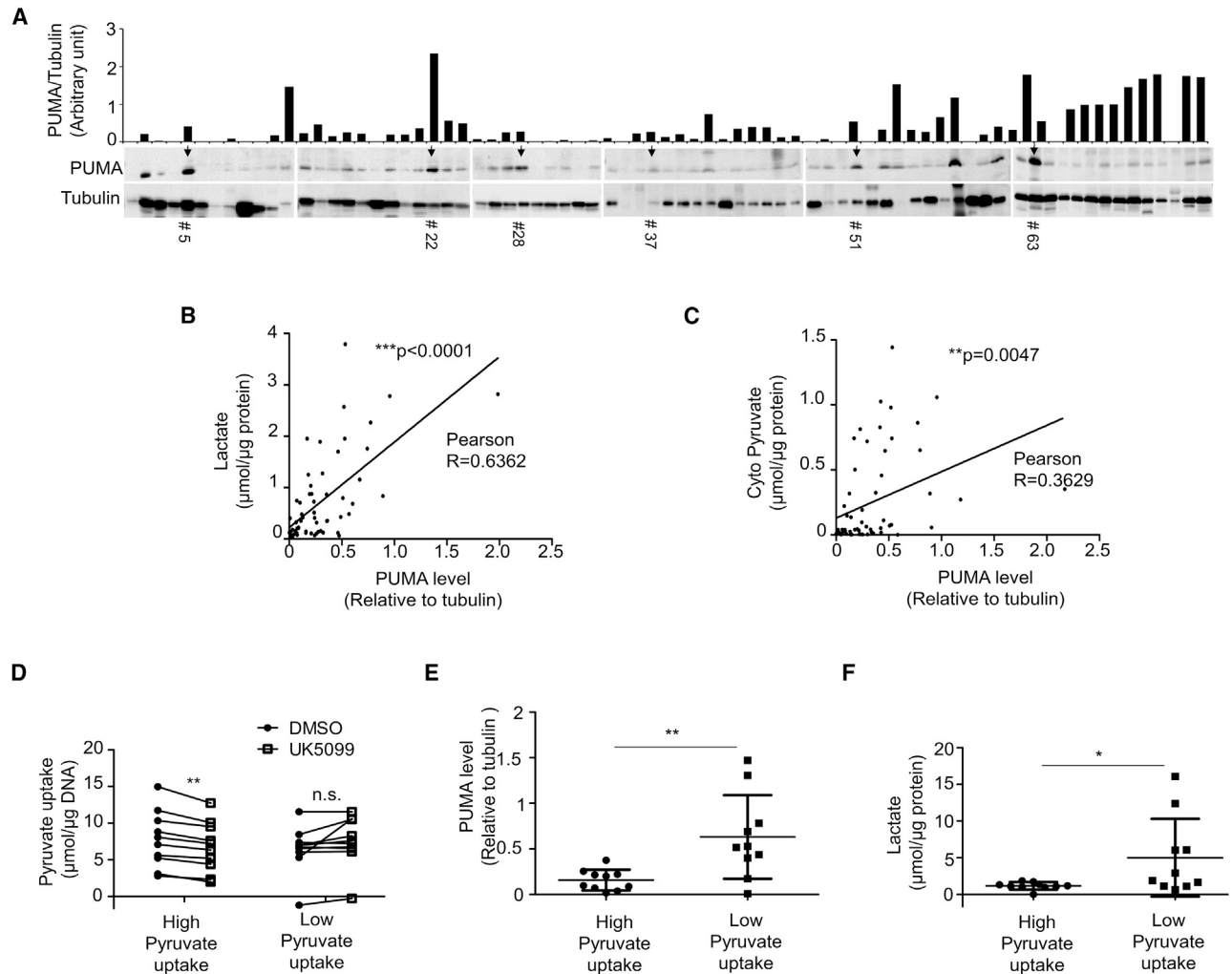


Figure 5. The Levels of PUMA Are Positively Correlated to Glycolytic Metabolism in HCC Derived from Cancer Patients

(A) The levels of PUMA protein in HCC samples were determined by western blotting analysis with anti-PUMA antibody. Tubulin was used as a loading control. Bar graph shows relative values of PUMA/tubulin in each sample. To standardize the PUMA/tubulin ratio throughout all blots, one sample from each blot (indicated by arrowheads) was loaded onto one gel and analyzed by western blotting.

(B and C) The correlation between the levels of PUMA in HCCs and the levels of lactate (B) and cytoplasmic pyruvate (C) in HCC. The levels of lactate and cytoplasmic pyruvate in individual samples were applied to the Pearson correlation test with the levels of PUMA in corresponding samples. The levels of PUMA were normalized to the levels of tubulin. $n = 59$ (15 HCC samples were excluded from analysis due to failure to detect PUMA or tubulin).

(D) MPC-dependent pyruvate uptake into mitochondria isolated from 20 HCC samples was measured by comparing the pyruvate levels in mitochondria with or without treatment with the MPC inhibitor UK5099 (0.2 mM). Based on levels of MPC-dependent pyruvate uptake, the HCC samples were divided into two groups: high and low mitochondrial pyruvate uptake.

(E and F) The correlation between the levels of PUMA (E) and lactate (F) in HCC samples with high or low MPC-dependent mitochondrial pyruvate uptake activity. $n = 10$ for each group.

Data are represented as mean \pm SD. Mann-Whitney test was used to calculate the statistical significance. * $p < 0.05$ and ** $p < 0.01$ denote significant differences. n.s., non-significant.

WTp53 could be important to maintain the genetic stability and homeostasis of adult stem cells, leading to the longer lifespan of mice with modestly elevated p53 activities. Therefore, this metabolic role of WTp53 could have opposite impacts on normal and cancer cells: it suppresses tumor initiation in normal cells but promotes tumorigenesis of cancer cells.

PUMA is a transcriptional target of p53 and is required for p53-dependent apoptosis, but the expression of PUMA can also be induced by a p53-independent mechanism (Sperka

et al., 2012). Considering that MPC function is critical for cellular survival (Vanderperre et al., 2016; Vigueira et al., 2014), the discovery of the roles of PUMA in suppressing MPC function provides another mechanism for PUMA-induced apoptosis. As the key mediator of p53-dependent apoptosis, PUMA has been predicted to be a tumor suppressor. In contrast to this assumption, PUMA is rarely mutated in human cancers, but instead overexpressed in many human cancers (Cai et al., 2013; Du et al., 2012; Kim et al., 2007; Sinicrope et al., 2008). The deficiency of

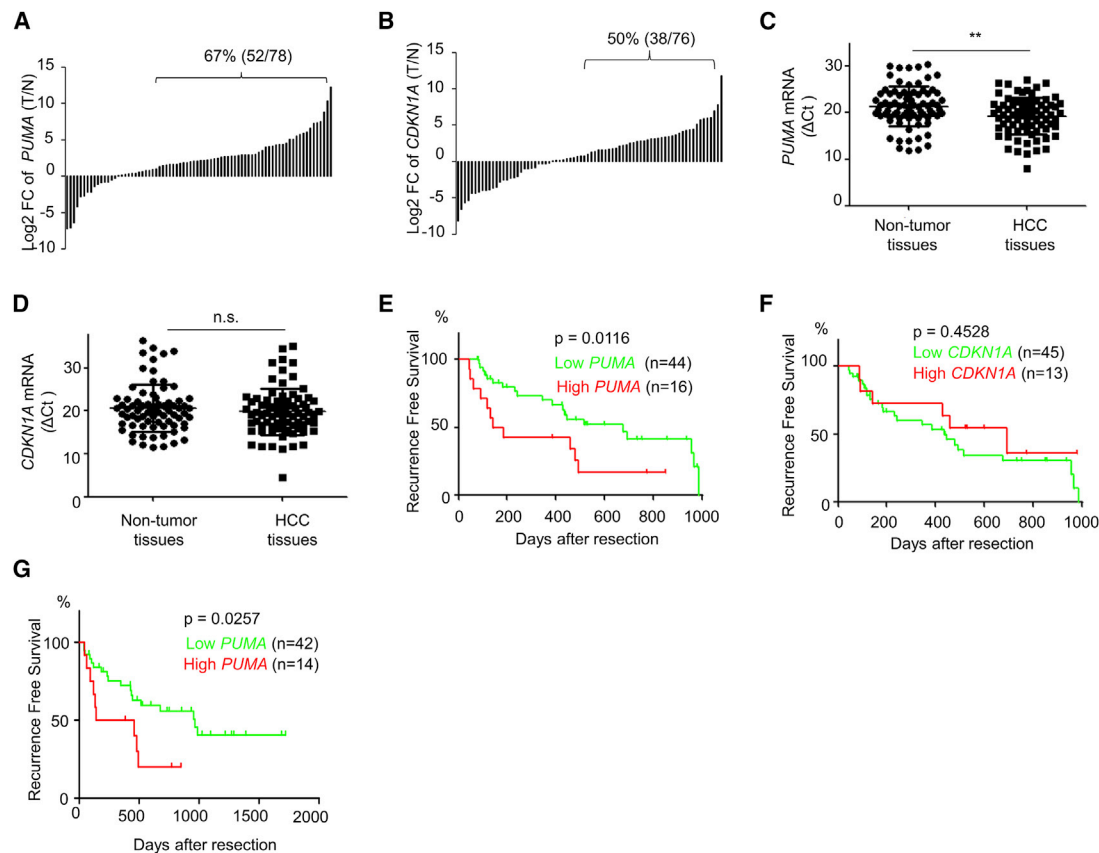


Figure 6. High Levels of PUMA Expression in HCC Are Positively Correlated to the Poor Prognosis of Cancer Patients

(A–D) Relative levels of *PUMA* (A) and *CDKN1A* (B) in the HCC tissue and the neighboring non-tumor tissue, and comparison of the levels of *PUMA* (C) and *CDKN1A* (D) in the group of HCC tissues and the neighboring non-tumor tissues. The levels of *PUMA* (n = 78) and *CDKN1A* (n = 76) mRNA in the pairs of HCC tissue and the neighboring non-tumor tissue are presented as log₂ of fold change (FC) of HCC tissue relative to neighboring non-tumor tissues (A and B) or compared in two groups (C and D). Data are represented as mean ± SD. Mann-Whitney test was used to calculate the statistical significance. **p < 0.01. n.s., non-significant.

(E and F) Log rank (Mantel Cox) survival test of HCC patients based on the levels of *PUMA* mRNA (n = 60, E) or *CDKN1A* mRNA (n = 58, F). The median survivals of the patients with high and low *PUMA* expression in HCCs are 162 and 675 days, respectively, while the median survivals of the patients with high and low *CDKN1A* expression in HCCs are 457 and 444 days, respectively.

(G) Log rank (Mantel Cox) survival test of HCC patients based on the levels of *PUMA* mRNA (n = 56) after the exclusion of the patients with *TP53* mutations.

PUMA prevents both irradiation-induced thymic lymphoma and chemically induced liver carcinoma in mice (Michalak et al., 2010; Qiu et al., 2011), suggesting that *PUMA* is an oncogene. The inactivation of MPC is known to suppress OXPHOS and promote glycolysis (Schell et al., 2014); our discovery of a key role of *PUMA* in shifting cellular metabolism from OXPHOS to glycolysis provides a mechanism to explain the roles of *PUMA* in promoting tumorigenesis.

IKKβ is oncogenic and promotes a cancer metabolic switch. Our data indicate that IKKβ-mediated phosphorylation of *PUMA* is important to activate *PUMA*'s function in suppressing MPC activity, and that *PUMA* mediates IKKβ-dependent suppression of OXPHOS. Therefore, the role of WTp53 in promoting the cancer metabolic switch is dependent on the activation of other oncogenic pathways such as IKKβ in cancer cells. Our findings also suggest that the expression levels of *PUMA* could dictate the roles of the p53-*PUMA* axis in apoptosis and metabolic switch in normal cells. In this context, the hyperactivation

of p53 induces high levels of *PUMA*, leading to apoptosis. In response to cellular stresses such as hypoxia, p53 is modestly activated to induce low levels of *PUMA*, leading to the metabolic switch from OXPHOS to glycolysis. In addition, *PUMA* can be upregulated in p53-independent manners in response to various stresses (Hikisz and Kiliańska, 2012), and thus can also promote the cancer metabolic switch in human cancer cells lacking functional p53. In further support of the important roles of *PUMA* in promoting tumorigenesis, our data indicate that the high expression levels of *PUMA* in HCC are positively correlated to the levels of glycolysis and poor prognosis of HCC patients.

Genetic instability is a hallmark of cancer, and cancer cells are under tremendous pressure to be selected for the pro-survival genetic mutations (Hanahan and Weinberg, 2011). Therefore, our discovery can explain the paradox in p53 biology that the WTp53 gene is retained in the majority of certain types of human cancer such as liver cancer. In this context, WTp53 appears to be important to maintain cancer metabolism in human cancer

Table 1. Univariate and Multivariate Cox Regression Analysis of Recurrence-Free Survival of HCC Patients

Variable	n	HR ^a	95% CI ^b	p
Univariate Analysis				
Age	45	0.438	0.162–1.184	0.104
<60 years	15			
≥60 years				
Gender	51	0.434	0.130–1.446	0.174
Male	9			
Female				
α-Fetoprotein	36	1.788	0.872–3.667	0.113
<400	24			
≥400				
Liver cirrhosis	49	1.245	0.456–3.397	0.668
Yes	11			
No				
Capsule	47	0.851	0.344–2.105	0.727
Yes	13			
No				
Tumor size	30	1.924	0.898–4.126	0.093
<5 cm	30			
≥5 cm				
Tumor number	53	2.837	1.073–7.498	0.035
1	7			
≥2				
Microvascular invasion (MVI)	32	5.577	2.372–13.114	0.000
Yes	28			
No				
Portal vein tumor thrombosis (PVTT)	14	2.496	1.167–5.337	0.018
46				
Yes				
No				
Differentiation	7	0.542	0.286–1.027	0.060
Well	40			
Moderate	13			
Poor				
Expression of PUMA	16	2.333	1.090–4.996	0.029
High	44			
Low				
Multivariate Analysis				
Tumor number		4.763	1.619–14.014	0.005
MVI (yes versus no)		2.212	1.065–4.595	0.033
PVTT (yes versus no)		0.710	0.289–1.743	0.454
PUMA expression (high versus low)		4.286	1.857–9.892	0.001

^aHazard ratio.

^bConfidence interval.

cells with higher OXPHOS activity such as HCC cells, but is dispensable for human cancer cells that have little mitochondrial activity and derive most of their energy from glycolysis. In summary, our findings have important implications for cancer diagnosis and therapy. For example, one of the intensively pursued strategies to eliminate human cancer is to either activate WTP53 in human cancers with small molecules such as RITA or restore WTP53 function to p53 mutants in human cancers harboring p53 mutations (Bykov et al., 2017; Song and Xu,

2007). In light of our findings, it is important to evaluate the metabolism of the human cancer that is selected for this therapy, because activation of WTP53 in human cancers could have a counterintuitive effect to promote tumorigenesis.

STAR★METHODS

Detailed methods are provided in the online version of this paper and include the following:

- KEY RESOURCES TABLE
- CONTACT FOR REAGENT AND RESOURCES SHARING
- EXPERIMENTAL MODEL AND SUBJECT DETAIL
 - HCC Patient Samples
 - Mice
 - Cell Culture, Lentivirus Production, and Transduction
- METHOD DETAILS
 - Vector Construction
 - Cell Growth Assay
 - Chemical and Cytokine Treatment
 - Mitochondria Isolation
 - Mitochondrial Pyruvate Uptake Assay
 - Measurement of ATP Levels
 - Measurement of Lactate Levels
 - FRET (Fluorescence Resonance Energy Transfer) Analysis
 - Confocal Microscopy
 - Western Blotting and Co-immunoprecipitation
 - Flow Cytometry
 - Total RNA Extraction and cDNA Synthesis
 - Quantitative PCR Analysis
 - Correlation Studies between PUMA Expression and Glycolysis of HCC Samples
 - Survival Correlation Studies on Patient Samples
 - Statistical Analysis

SUPPLEMENTAL INFORMATION

Supplemental Information includes five figures and one table and can be found with this article online at <https://doi.org/10.1016/j.ccell.2018.12.012>.

ACKNOWLEDGMENTS

We thank Professor D.H. Yang for HCC tissue samples and clinical data, Nicole G. Nalbandian and Michael Qu for technical support, and Dr. Zambetti for PUMA knockout mice. This study was supported by the National Natural Science Foundation of China (8153000450, 81871197, 81430032, U1601222), the Leading Talents of Guangdong Province Program (00201516), the National High-Tech R&D Program (863 Program 2015AA020310), the Major Basic Research Developmental Project of the Natural Science Foundation of Guangdong Province, Development and Reform Commission of Shenzhen Municipality (S2016004730009), the Sanming Project of Medicine in Shenzhen (SZSM201602102), the South Wisdom Valley Innovative Research Team Program (2014) 365, and the California Institute for Regenerative Medicine (TR1-01277).

AUTHOR CONTRIBUTIONS

Conceptualization: J.K., L.Y., X.F., and Yang Xu; Methodology: J.K., L.Y., X.F., and Yang Xu; Investigation: J.K., L.Y., M.W., Yanxia Xu, W.C., D.T., Q.T., B.F., L.J., and J.H.; Formal Analysis: J.K., L.Y., X.F., and Yang Xu; Resources: G.C.; Writing – Original Draft: J.K. and Yang Xu; Writing – Review and Editing: all

authors; Supervision: X.F. and Yang Xu; Project Administration: X.F. and Yang Xu; Funding Acquisition: X.F. and Yang Xu.

DECLARATION OF INTERESTS

The authors declare no competing interests.

Received: March 28, 2018

Revised: December 4, 2018

Accepted: December 27, 2018

Published: January 31, 2019

REFERENCES

- Brugarolas, J., Chandrasekaran, C., Gordon, J.I., Beach, D., Jacks, T., and Hannon, G.J. (1995). Radiation-induced cell cycle arrest compromised by p21 deficiency. *Nature* *377*, 552–557.
- Bykov, V.J.N., Eriksson, S.E., Bianchi, J., and Wiman, K.G. (2017). Targeting mutant p53 for efficient cancer therapy. *Nat. Rev. Cancer* *18*, 89–102.
- Cai, W., Li, Q., Yang, Z., Miao, X., Wen, Y., Huang, S., and Ouyang, J. (2013). Expression of p53 upregulated modulator of apoptosis (PUMA) and C-myc in gallbladder adenocarcinoma and their pathological significance. *Clin. Transl. Oncol.* *15*, 818–824.
- Chao, C., Herr, D., Chun, J., and Xu, Y. (2006). Ser18 and 23 phosphorylation is required for p53-dependent apoptosis and tumor suppression. *EMBO J.* *25*, 2615–2622.
- Chao, C., Saito, S., Anderson, C.W., Appella, E., and Xu, Y. (2000). Phosphorylation of murine p53 at ser-18 regulates the p53 responses to DNA damage. *Proc. Natl. Acad. Sci. U S A* *97*, 11936–11941.
- Craig, A.L., Burch, L., Vojtesek, B., Mikutowska, J., Thompson, A., and Hupp, T.R. (1999). Novel phosphorylation sites of human tumour suppressor protein p53 at Ser20 and Thr18 that disrupt the binding of MDM2 (mouse double minute 2) protein are modified in human cancers. *Biochem. J.* *342*, 133–141.
- Deng, C., Zhang, P., Harper, J.W., Elledge, S.J., and Leder, P. (1995). Mice lacking p21CIP1/WAF1 undergo normal development, but are defective in G1 checkpoint control. *Cell* *82*, 675–684.
- Du, Q.H., Zhang, K.J., Jiao, X.L., Zhao, J., Zhang, M., Yan, B.M., and Xu, Y.B. (2012). Prognostic significance of PUMA in pancreatic ductal adenocarcinoma. *J. Int. Med. Res.* *40*, 2066–2072.
- Fricker, M., O'Prey, J., Tolkovsky, A.M., and Ryan, K.M. (2010). Phosphorylation of PUMA modulates its apoptotic function by regulating protein stability. *Cell Death Dis.* *1*, e59.
- Fu, X., Cui, K., Yi, Q., Yu, L., and Xu, Y. (2017). DNA repair mechanisms in embryonic stem cells. *Cell. Mol. Life Sci.* *74*, 487–493.
- Garcia-Cao, I., Garcia-Cao, M., Martin-Caballero, J., Criado, L.M., Klatt, P., Flores, J.M., Weill, J.C., Blasco, M.A., and Serrano, M. (2002). "Super p53" mice exhibit enhanced DNA damage response, are tumor resistant and age normally. *EMBO J.* *21*, 6225–6235.
- Hanahan, D., and Weinberg, R.A. (2011). Hallmarks of cancer: the next generation. *Cell* *144*, 646–674.
- Herzig, S., Raemy, E., Montessuit, S., Veuthey, J.L., Zamboni, N., Westermann, B., Kunji, E.R., and Martinou, J.C. (2012). Identification and functional expression of the mitochondrial pyruvate carrier. *Science* *337*, 93–96.
- Hikisz, P., and Kiliariska, Z. (2012). PUMA, a critical mediator of cell death—one decade on from its discovery. *Cell. Mol. Biol. Lett.* *17*, 646–669.
- Humpton, T.J., and Vousden, K.H. (2016). Regulation of cellular metabolism and hypoxia by p53. *Cold Spring Harb. Perspect. Med.* *6*, <https://doi.org/10.1101/cshperspect.a026146>.
- Issaeva, N., Bozko, P., Enge, M., Protopopova, M., Verhoef, L.G.G.C., Masucci, M., Pramanik, A., and Selivanova, G. (2004). Small molecule RITA binds to p53, blocks p53-HDM-2 interaction and activates p53 function in tumors. *Nat. Med.* *10*, 1321–1328.
- Jeffers, J.R., Parganas, E., Lee, Y., Yang, C., Wang, J., Brennan, J., MacLean, K.H., Han, J., Chittenden, T., Ihle, J.N., et al. (2003). PUMA is an essential mediator of p53-dependent and -independent apoptotic pathways. *Cancer Cell* *4*, 321–328.
- Jiang, D., Brady, C.A., Johnson, T.M., Lee, E.Y., Park, E.J., Scott, M.P., and Attardi, L.D. (2011). Full p53 transcriptional activation potential is dispensable for tumor suppression in diverse lineages. *Proc. Natl. Acad. Sci. U S A* *108*, 17123–17128.
- Kastenhuber, E.R., and Lowe, S.W. (2017). Putting p53 in context. *Cell* *170*, 1062–1078.
- Kim, J., Nakasaki, M., Todorova, D., Lake, B., Yuan, C.Y., Jamora, C., and Xu, Y. (2014). p53 induces skin aging by depleting Blimp1+ sebaceous gland cells. *Cell Death Dis.* *5*, e1141.
- Kim, M.R., Jeong, E.G., Chae, B., Lee, J.W., Soung, Y.H., Nam, S.W., Lee, J.Y., Yoo, N.J., and Lee, S.H. (2007). Pro-apoptotic PUMA and anti-apoptotic phospho-BAD are highly expressed in colorectal carcinomas. *Dig. Dis. Sci.* *52*, 2751–2756.
- Kruiswijk, F., Labuschagne, C.F., and Vousden, K.H. (2015). p53 in survival, death and metabolic health: a lifeguard with a licence to kill. *Nat. Rev. Mol. Cell Biol.* *16*, 393–405.
- Lake, B.B., Fink, J., Klemetsaune, L., Fu, X., Jeffers, J.R., Zambetti, G.P., and Xu, Y. (2012). Context-dependent enhancement of induced pluripotent stem cell reprogramming by silencing PUMA. *Stem Cells* *30*, 888–897.
- Le-yang, X., Huo-hui, O., Xin-cheng, L., Zhan-jun, C., Xiang-hong, L., Yu, H., and Ding-hua, Y. (2017). Loss of tumor suppressor miR-126 contributes to the development of hepatitis B virus-related hepatocellular carcinoma metastasis through the upregulation of ADAM9. *Tumor Biol.* *39*, 1010428317709128.
- Li, T., Kon, N., Jiang, L., Tan, M., Ludwig, T., Zhao, Y., Baer, R., and Gu, W. (2012). Tumor suppression in the absence of p53-mediated cell-cycle arrest, apoptosis, and senescence. *Cell* *149*, 1269–1283.
- Lin, T., Chao, C., Saito, S., Mazur, S.J., Murphy, M.E., Appella, E., and Xu, Y. (2005). p53 induces differentiation of mouse embryonic stem cells by suppressing Nanog expression. *Nat. Cell Biol.* *7*, 165–171.
- Liu, D., Ou, L., Clemenson, G.D., Jr., Chao, C., Lutske, M.E., Zambetti, G.P., Gage, F.H., and Xu, Y. (2010). PUMA is required for p53-induced depletion of adult stem cells. *Nat. Cell Biol.* *12*, 993–998.
- Liu, G., Parant, J.M., Lang, G., Chau, P., Chavez-Reyes, A., El-Naggar, A.K., Multani, A., Chang, S., and Lozano, G. (2004). Chromosome stability, in the absence of apoptosis, is critical for suppression of tumorigenesis in Trp53 mutant mice. *Nat. Genet.* *36*, 63–68.
- Matheu, A., Maraver, A., Klatt, P., Flores, I., Garcia-Cao, I., Borrás, C., Flores, J.M., Vina, J., Blasco, M.A., and Serrano, M. (2007). Delayed ageing through damage protection by the Arf/p53 pathway. *Nature* *448*, 375–379.
- Meek, David W. (2015). Regulation of the p53 response and its relationship to cancer. *Biochem. J.* *469*, 325–346.
- Mello, S.S., and Attardi, L.D. (2018). Deciphering p53 signaling in tumor suppression. *Curr. Opin. Cell Biol.* *51*, 65–72.
- Mendrysa, S.M., O'Leary, K.A., McElwee, M.K., Michalowski, J., Eisenman, R.N., Powell, D.A., and Perry, M.E. (2006). Tumor suppression and normal aging in mice with constitutively high p53 activity. *Genes Dev.* *20*, 16–21.
- Michalak, E.M., Vandenberg, C.J., Delbridge, A.R., Wu, L., Scott, C.L., Adams, J.M., and Strasser, A. (2010). Apoptosis-promoted tumorigenesis: gamma-irradiation-induced thymic lymphomagenesis requires PUMA-driven leukocyte death. *Genes Dev.* *24*, 1608–1613.
- Murphy, M., Hinman, A., and Levine, A.J. (1996). Wild-type p53 negatively regulates the expression of a microtubule-associated protein. *Genes Dev.* *10*, 2971–2980.
- Prokesch, A., Graef, F.A., Madl, T., Kahlhofer, J., Heidenreich, S., Schumann, A., Moyschewitz, E., Pristoynik, P., Blaschitz, A., Knauer, M., et al. (2016). Liver p53 is stabilized upon starvation and required for amino acid catabolism and gluconeogenesis. *FASEB J.* *31*, 732–742.
- Qiu, W., Wang, X., Leibowitz, B., Yang, W., Zhang, L., and Yu, J. (2011). PUMA-mediated apoptosis drives chemical hepatocarcinogenesis in mice. *Hepatology* *54*, 1249–1258.

- Rong, Z., Zhu, S., Xu, Y., and Fu, X. (2014). Homologous recombination in human embryonic stem cells using CRISPR/Cas9 nickase and a long DNA donor template. *Protein Cell* 5, 258–260.
- Roszik, J., Szollosi, J., and Vereb, G. (2008). AccPbFRET: an ImageJ plugin for semi-automatic, fully corrected analysis of acceptor photobleaching FRET images. *BMC Bioinformatics* 9, 346.
- Saito, S., Yamaguchi, H., Higashimoto, Y., Chao, C., Xu, Y., Fornace, A.J., Jr., Appella, E., and Anderson, C.W. (2003). Phosphorylation site interdependence of human p53 post-translational modifications in response to stress. *J. Biol. Chem.* 278, 37536–37544.
- Schell, J.C., Olson, K.A., Jiang, L., Hawkins, A.J., Van Vranken, J.G., Xie, J., Egnatchik, R.A., Earl, E.G., DeBerardinis, R.J., and Rutter, J. (2014). A role for the mitochondrial pyruvate carrier as a repressor of the Warburg effect and colon cancer cell growth. *Mol. Cell* 56, 400–413.
- Shen, L., Sun, X., Fu, Z., Yang, G., Li, J., and Yao, L. (2012). The fundamental role of the p53 pathway in tumor metabolism and its implication in tumor therapy. *Clin. Cancer Res.* 18, 1561–1567.
- Shieh, S.Y., Ahn, J., Tamai, K., Taya, Y., and Prives, C. (2000). The human homologs of checkpoint kinases Chk1 and Cds1 (Chk2) phosphorylate p53 at multiple DNA damage-inducible sites. *Genes Dev.* 14, 289–300.
- Sinicrope, F.A., Rego, R.L., Okumura, K., Foster, N.R., O'Connell, M.J., Sargent, D.J., and Windschitl, H.E. (2008). Prognostic impact of bim, PUMA, and noxa expression in human colon carcinomas. *Clin. Cancer Res.* 14, 5810–5818.
- Song, H., and Xu, Y. (2007). Gain of function of p53 cancer mutants in disrupting critical DNA damage response pathways. *Cell Cycle* 6, 1570–1573.
- Soussi, T., and Wiman, K.G. (2007). Shaping genetic alterations in human cancer: the p53 mutation paradigm. *Cancer Cell* 12, 303–312.
- Sperka, T., Wang, J., and Rudolph, K.L. (2012). DNA damage checkpoints in stem cells, ageing and cancer. *Nat. Rev. Mol. Cell Biol.* 13, 579–590.
- Tornatore, L., Thotakura, A.K., Bennett, J., Moretti, M., and Franzoso, G. (2012). The nuclear factor kappa B signaling pathway: integrating metabolism with inflammation. *Trends Cell Biol.* 22, 557–566.
- Vanderperre, B., Herzig, S., Krznar, P., Horl, M., Ammar, Z., Montessuit, S., Pierredon, S., Zamboni, N., and Martinou, J.C. (2016). Embryonic lethality of mitochondrial pyruvate carrier 1 deficient mouse can be rescued by a ketogenic diet. *PLoS Genet.* 12, e1006056.
- Vigueira, P.A., McCommis, K.S., Schweitzer, G.G., Remedi, M.S., Chambers, K.T., Fu, X., McDonald, W.G., Cole, S.L., Colca, J.R., Kletzien, R.F., et al. (2014). Mitochondrial pyruvate carrier 2 hypomorphism in mice leads to defects in glucose-stimulated insulin secretion. *Cell Rep.* 7, 2042–2053.
- Villunger, A., Michalak, E.M., Coultas, L., Mullaer, F., Bock, G., Ausserlechner, M.J., Adams, J.M., and Strasser, A. (2003). p53- and drug-induced apoptotic responses mediated by BH3-only proteins PUMA and noxa. *Science* 302, 1036–1038.
- Vousden, K.H., and Prives, C. (2009). Blinded by the light: the growing complexity of p53. *Cell* 137, 413–431.
- Wade, M., Li, Y.-C., and Wahl, G.M. (2013). MDM2, MDMX and p53 in oncogenesis and cancer therapy. *Nat. Rev. Cancer* 13, 83–96.
- Wilfling, F., Weber, A., Potthoff, S., Vogtle, F.N., Meisinger, C., Paschen, S.A., and Hacker, G. (2012). BH3-only proteins are tail-anchored in the outer mitochondrial membrane and can initiate the activation of Bax. *Cell Death Differ.* 19, 1328–1336.
- Xu, Y. (2003). Regulation of p53 responses by post-translational modifications. *Cell Death Differ.* 10, 400–403.
- Xu, Y. (2008). Induction of genetic instability by gain-of-function p53 cancer mutants. *Oncogene* 27, 3501–3507.
- Xue, Y., Zhou, F., Zhu, M., Ahmed, K., Chen, G., and Yao, X. (2005). GPS: a comprehensive www server for phosphorylation sites prediction. *Nucleic Acids Res.* 33, W184–W187.

STAR★METHODS

KEY RESOURCES TABLE

REAGENT or RESOURCE	SOURCE	IDENTIFIER
Antibodies		
Mouse monoclonal anti-PUMA (G-3)	Santa Cruz	Cat# sc-374223; RRID: AB_10987708
Rabbit polyclonal anti-PUMA (H-136)	Santa Cruz	Cat# sc-28226; RRID: AB_2064827
Rabbit polyclonal anti-PUMA (D30C10)	Cell signaling	Cat# 12450
Goat polyclonal anti-PUMA	Novus	Cat# NBP1-52093; RRID: AB_11027545
Mouse monoclonal anti-Flag M2	Sigma Aldrich	Cat# F1804; RRID: AB_262044
Rabbit polyclonal anti-GFP (FL)	Santa Cruz	Cat# sc-8334; RRID: AB_641123
Mouse monoclonal anti-GFP (B-2)	Santa Cruz	Cat# sc-28226; RRID: AB_2064827
Rabbit polyclonal anti-phospho serine	Abcam	Cat# ab9332; RRID: AB_307184
Rabbit polyclonal anti-IKK β (L570)	Cell signaling	Cat# 2678; RRID: AB_2122301
Rabbit polyclonal anti-phospho-IKK β (C84E11)	Cell signaling	Cat# 2078; RRID: AB_2097379
Rabbit monoclonal anti-MPC1 (D2L9I)	Cell signaling	Cat# 14462
Rabbit monoclonal anti-MPC2 (D4I7G)	Cell signaling	Cat# 46141
Rabbit polyclonal anti-MPC1	Novus	Cat# NBP1-91706; RRID: AB_11035008
Mouse monoclonal anti- α -Tubulin (B-5-1-2)	Santa Cruz	Cat# Cat# sc-23948; RRID: AB_628410
Mouse monoclonal anti- α -Tubulin (B-5-1-2)	Sigma Aldrich	Cat# T5168; RRID: AB_477579
Anti-rabbit IgG, HRP-linked antibody	Cell signaling	Cat# 7074S; RRID: AB_2099233
Anti-mouse IgG, HRP-linked antibody	Cell signaling	Cat# 7076S; RRID: AB_330924
Alexa Fluor 488-Donkey anti-rabbit	Thermo scientific	Cat# A21206; RRID: AB_2535792
Alexa Fluor 568-Donkey anti-goat	Thermo scientific	Cat# A11057; RRID: AB_142581
Bacterial and Virus Strains		
E.coli. Stable Competent cells	NEB	Cat# C3040H
E.coli. Top10 competent cells	Thermo scientific	Cat# C404010
E.coli. Stbl3 competent cells	Thermo scientific	Cat# C737303
Biological Samples		
Human liver cancer tissues	(Le-yang et al., 2017)	N/A
Mouse tissues	(Liu et al., 2010)	N/A
Chemicals, Peptides, and Recombinant Proteins		
Matrigel Matrix	Corning	Cat# 354277
TNF- α	Peptotech	Cat# 300-01A
Halt protease & phosphatase inhibitor cocktail	Thermo Scientific	Cat#78440
UK5099	Sigma Aldrich	Cat# PZ0160
Oligomycin	Sigma Aldrich	Cat# O4876
IKK16	Selleckchem	Cat# S2882
TPCA-1	Selleckchem	Cat# S2824
2-DG	Sigma Aldrich	Cat# D8375
RITA	Selleckchem	Cat# S2781
Doxycycline	Sigma Aldrich	Cat# D3072
Lipofectamine 2000	Thermo scientific	Cat# 11668019
Pyruvic acid	Sigma Aldrich	Cat# 107360
ADP	Sigma Aldrich	Cat# A2754
Malic acid	Sigma Aldrich	Cat# M0875
Lenti-X concentrator	Takara Bio	Cat# 631232
Polybrene	Millipore	Cat# TR-1003-G
Puromycin	Gibco	Cat# A1113803

(Continued on next page)

Continued

REAGENT or RESOURCE	SOURCE	IDENTIFIER
FluoroBrite™ DMEM	Thermo Scientific	Cat# A1896701
Critical Commercial Assays		
Pyruvate measurement kit	Cayman	Cat# 700470
Pyruvate measurement kit	Biovision	Cat# K609
Lactate measurement kit	Biovision	Cat# 607
PicoProbe Lactate Fluorometric Assay kit	Biovision	Cat# 638
ATP measurement kit	PerkinElmer	Cat# 6016941
Mitochondrial isolation kit	Thermo Scientific	Cat# 89874
Mitochondria protein IP kit	Sigma Aldrich	Cat# MTP001
BCA kit	Sigma Aldrich	Cat# BCA1 AND B9643
Annexin V kit	Thermo scientific	Cat# BMS500FI
CCK-8 kit	Dojindo	Cat# CK04-05
Quant-iT PicoGreen dsDNA Reagent	Thermo Scientific	Cat# P7589
Deposited Data		
TetO-Fuw PGK-puro	This study	Genbank accession No. MK318529
p2U6-CAG-Cas9-p2A-puro	This study	Genbank accession No. MK318530
Experimental Models: Cell Lines		
HEK 293 FT cell	Thermo scientific	Cat# R70007
HepG2	ATCC	Cat# HB-8065
LS 174T	ATCC	CL-188
HCT116	ATCC	CCL247
A549	ATCC	CRM-CCL-185
HeLa	ATCC	CCL-2
Ca Ski	ATCC	CRL-1550
MCF7	ATCC	HTB-22
RKO	ATCC	CRL-2577
LoVo	ATCC	CCL-229
SK-Hep1	Cell Resource Center, Chinese Academy of Science	3111C0001ccc000677
BEL7404	Cell Resource Center, Chinese Academy of Science	3131C0001000700064
SMMC7721	Cell Resource Center, Chinese Academy of Science	3142C0001000000063
Experimental Models: Organisms/Strains		
Mouse: NOD.CB17-Prkdc ^{scid} /J	Jackson Laboratory	Stock#: 001303
Mouse: NSG	Jackson Laboratory	Stock#: 005557
Mouse: <i>Trp53</i> ^{TSD/-}	(Liu et al., 2010)	N/A
Mouse: <i>Trp53</i> ^{+/-} ,	(Liu et al., 2010)	N/A
Mouse: <i>Trp53</i> ^{+/-} <i>Puma</i> ^{-/-}	(Liu et al., 2010)	N/A
Mouse: <i>Trp53</i> ^{TSD/-} <i>Puma</i> ^{-/-}	(Liu et al., 2010)	N/A
Oligonucleotides		
Primers for qRT-PCR	This study	See Table S1
Primers for cloning	This study	See Table S1
Oligomers for shRNA	This study	See Table S1
Oligomers for gRNA	This study	See Table S1
Recombinant DNA		
pcDNA3-PUMA α -Flag3x	This study	N/A
pcDNA3-PUMA β -Flag3x	This study	N/A
pcDNA3-PUMA 2A-Flag3x	This study	N/A

(Continued on next page)

Continued

REAGENT or RESOURCE	SOURCE	IDENTIFIER
eGFP N1-PUMA α	This study	N/A
mCherry N1-PUMA α	This study	N/A
mCherry N1-PUMA del92	This study	N/A
mCherry N1-PUMA del137	This study	N/A
mCherry N1-PUMA delBH3	This study	N/A
pLenti-CMV mCherry-PUMA α	This study	N/A
pLenti-CMV mCherry-PUMA del92	This study	N/A
pLenti-CMV mCherry-PUMA del137	This study	N/A
pLenti-CMV mCherry-PUMA delBH3	This study	N/A
TetOn-pLKO1-shp53 PUMA	This study	N/A
pLKO1-shPUMA	This study	N/A
pLKO1-shP21	This study	N/A
pLKO1-shp53#1	Addgene	Cat# 19119
pLKO1-shp53#2	This study	N/A
pLKO1-scram	This study	N/A
TetO-Fuw- PUMA α -Flag3x PGK-puro	This study	N/A
TetO-Fuw- PUMA 2A-Flag3x PGK-puro	This study	N/A
TetO-Fuw- PUMA delBH3-Flag3x PGK-puro	This study	N/A
TetO-Fuw-control-PGK-puro	This study	N/A
p2U6-gRNA PUMA-CAG-Cas9-puro	This study	N/A
pcDNA-IKKb-FLAG-WT	Addgene	Cat# 23298
psPAX2	Addgene	Cat# 12260
pMD2.G	Addgene	Cat# 12259
Fuw-M2rtTA	Addgene	Cat# 20342
eGFPN1-MPC1	This study	N/A
eGFPN1-MPC2	This study	N/A
mCherryN1-MPC2	This study	N/A
Software and Algorithms		
FlowJo	FLOWJO, LLC	N/A
ImageJ	NIH	https://imagej.nih.gov/ij/
GraphPad Prism	GraphPad software	N/A
AccPbFRET plugin	(Roszik et al., 2008)	https://github.com/camlloyd/AccPbFRET
Colocalization colormap plugin		https://sites.google.com/site/colocalizationcolormap/home
Image Lab	BioRad	N/A
GSP 3.0	(Xue et al., 2005)	http://gps.biocuckoo.org/

CONTACT FOR REAGENT AND RESOURCES SHARING

Further information and request for resources and reagents should be directed to and will be fulfilled by the Lead contact, Yang Xu (yangxu@ucsd.edu).

EXPERIMENTAL MODEL AND SUBJECT DETAIL

HCC Patient Samples

All patient related studies were approved by the Institutional Review Board of Nanfang Hospital of Southern Medical University. As previously described (Le-yang et al., 2017), after obtaining adequate informed consent from patients, hepatocellular carcinoma (HCC) tissues and adjacent normal tissues (ANT, exceeding the edge of the tumor by at least 2 cm) were obtained from HCC patients who underwent curative resection in the Department of Hepatobiliary Surgery, Nanfang Hospital of Southern Medical University, Guangzhou, China. Patients were monitored for further survival analysis via outpatient follow-up and telephone interviews. A relapse

was confirmed based on increased post-operative blood alpha-fetoprotein (AFP) levels and imaging tests (ultrasonic examination, computed tomography scan, or magnetic resonance imaging).

Mice

All animal work was approved by Institutional Animal Care and Use Committee (IACUC) of Southern Medical University and University of California, San Diego. To examine tumor formation in male NODSCID or NSG mice, 5×10^6 cells were resuspended in 0.2 ml serum-free DMEM with 50% matrigel (Corning) and injected subcutaneously into the flanks of 2- to 3-month-old mice. Mice were killed 3 to 8 weeks after implantation, and tumors excised and weighted. For the inducible knockdown *in vivo*, NSG mice bearing established tumors about 0.5cm in diameter were separated into two groups, one group was injected intraperitoneally (i.p.) with Doxy (20 mg/kg body weight) every day and provided with water supplemented with Doxy (2 mg/L). The control group was injected with the same volume of PBS. Tumor size was measured using caliper and calculated using formula $V = (W(2) \times L)/2$, where V is tumor's volume, W is tumor's width, L is tumor's length. When the mice were sacrificed, all tumors were collected, weighted, and photographed. *Trp53*^{TSD/+} mice and PUMA KO mice were maintained as previously described (Liu et al., 2010). Livers of 4-5-week-old male mice were analyzed for metabolic parameters.

Cell Culture, Lentivirus Production, and Transduction

HEK 293 FT cell line was purchased from Thermo Scientific. Other cell lines were obtained from ATCC (American Type Culture Collection) and Cell Resource Center of Chinese Academy of Science. All cell lines were cultured in DMEM (Gibco) supplemented with 10% fetal bovine serum (FBS) (Hyclone) and 1% Penicillin-Streptomycin (Pen/Strep) (Gibco) at 37°C with 5% CO₂.

Plasmid DNA for transfection and lentivirus packaging was purified with NucleoBond Xtra Maxi EF kits (Takara Bio) or EndoFree Plasmid Maxi Kit (Qiagen) according to the manufacturer's instruction. Transfection was performed using Lipofectamine 2000 reagent (Thermo scientific) according to manufacturer's protocol. For lentivirus production, PEI method was used according to Addgene's lentivirus production protocol with minor modifications. One day after confluent 293FT packaging cells were plated onto 15 cm dishes at an 1:3 dilution, two packaging plasmids psPAX2 (Addgene 12260) and pMD2.G (Addgene 12259) together with either Fuv-TetO-based transfer plasmids or pLKO-based transfer plasmids were diluted in Opti-MEM (Gibco) with 1 mg/ml PEI at the DNA:PEI ratio of 1:3-1:4. Plasmid mixtures were transfected into cells and media replaced with complete DMEM 16 hr after transfection. Lentivirus was harvested 72 hr post transfection using Lenti-X concentrator (Takara Bio) according to manufacturer's instruction. When using TetO-Fuv based system, cells were co-infected with lentivirus harboring Fuv-M2rtTA (Addgene 20342) for the doxycycline (Doxy)-inducible expression. Collected media was centrifuged at 500 × g for 10 min and supernatant incubated with 1/3 volume of Lenti-X Concentrator overnight. After centrifugation at 1500 × g for 45 minutes at 4°C, viral pellets were resuspended in 0.4-0.8 ml PBS and stored at -80°C.

Lentivirus transduction was performed accordingly to Addgene PLKO.1 protocol. To establish stable knockdown cells, pLKO.1 puro lentiviral vector (Addgene 8453) was used to express short hairpin RNA (shRNA). For the Doxy-inducible p53 knockdown, the lentiviral vector tet-pLKO-puro vector (Addgene 21915) was used to express the shRNA inducibly. We repeated the experiments with two distinct p53 shRNA target sequences (Table S1). The sequences of shRNAs targeting *PUMA* and *p21* are listed in Table S1. After transduction, cells were selected with puromycin (2 μg/ml) and subsequently treated with 1 μg/ml of Doxy to induce the expression of shRNA.

CRISPR/Cas9-gRNA system was used to knockout *PUMA* in HepG2 cells. P2U6-PUMA gRNA CAG-puro plasmids expressing CAS9 and two gRNAs targeting adjacent regions of *PUMA* exons (Table S1) were transfected into HepG2 cells using Lipofectamine 2000 according to manufacturer's instruction. Transfected cells were selected with 2 μg/ml of puromycin for 3 days. Single colonies were expanded and screened for *PUMA* knockout by Western blotting analysis of *PUMA* expression. The positive clones were confirmed by amplification and sequencing of the genomic region targeted by the gRNAs. The PCR and sequencing primers are listed in Table S1.

To restore the expression of WT and *PUMA* mutants in *PUMA* KO cells, *PUMA* KO cells were transduced with lentivirus harboring inducible expression cassettes for *PUMA* (TetO-Fuv-*PUMA*_α-PGK-puro) or *PUMA* mutants (TetO-Fuv-*PUMA*_Δ1B3-PGK-puro and TetO-Fuv-*PUMA* 2A-PGK-puro) or control plasmid (TetO-Fuv-control-PGK-puro). Lentivirus harboring Fuv-M2rtTA for the inducible expression of transcriptional activator was co-transduced into the cells. Three days after transduction, cells were selected with 2 μg/ml puromycin for 2 days and analyzed.

METHOD DETAILS

Vector Construction

To generate plasmids expressing human MPC1 or MPC2, the full-length cDNA was inserted into mCherry N1 (Cloneteck 632523) and eGFPN1 vectors (Cloneteck 6085-1) through restriction enzyme sites HindIII and BamHI. The full-length cDNA was amplified by PCR from the cDNA from HUES human embryonic stem cells using Q5 High-Fidelity DNA Polymerase (NEB). To obtain vectors expressing two human *PUMA* isoforms, full-length cDNA for two isoforms was amplified by PCR with an addition of 3x Flag sequences at C-terminus and cloned into pcDNA3 vector. For tagging fluorescence to proteins, the full-length cDNA was inserted into mCherry N1 through restriction enzyme sites HindIII and BamHI. The cDNAs encoding the deletional mutants of *PUMA* and phosphorylation site mutant *PUMA* were generated by PCR. Sequences of all primers used in the PCR-based cloning were provided in Table S1. For

the tagging of mCherry to the N-terminus of PUMA, Gibson assembly (NEBuilder HiFi DNA Assembly Master Mix) was performed with PCR products of mCherry, various PUMA cDNA, and pLenti-CMV-GFP vector (Addgene 17448) linearized by BamHI/SalI digestion. To construct plasmids that express genes inducibly, cDNAs for PUMA or various mutant forms of PUMA were used for Gibson assembly with TetO-Fuw-PGK-puro vector modified from tetO Fuw-OSKM vector (Addgene plasmid 20321) linearized by EcoRI/Agel digestion. In the modified vector, OSKM was removed by EcoRI digestion and NheI site added after the EcoRI site. PGK-puro selection cassette was inserted into Agel and NheI sites, resulting in TetO-Fuw PGK-puro. The sequence of TetO-Fuw PGK-puro is deposited in GenBank with the accession number MK318529.

CRISPR web based-design tool (<http://crispr.mit.edu>) was used for designing gRNAs for PUMA knockout. gRNA oligomers were designed to complement the sticky end sequences after BclI digestion of p2U6-CAG-Cas9-p2A-puro plasmid, which was modified from p2U6-CAG-Cas9-p2A-mCherry vector (Rong et al., 2014) by replacing cDNA encoding for mCherry with that for puromycin resistance gene. The sequence of p2U6-CAG-Cas9-p2A-puro is deposited into GenBank with the accession number MK318530.

Cell Growth Assay

For the clonogenic assay of human cancer cell lines, single cell suspension was prepared by trypsinization and cells seeded onto 6-well plates at a density of 2000 cells per well. Colonies of cells were fixed with cold methanol, stained with 0.1% crystal violet, and counted. Cellular proliferation was determined with cell Counting Kit 8 assay (CCK8, Dojindo) according to the manufacturer's protocol. Briefly, twelve cancer cell lines with inducible p53 knockdown vector were incubated with or without 1 μ g/ml of Doxy for 3 days, and subsequently seeded in 96-well plates at a density of 3×10^3 cells/well. At different time points (24–96 hours) after plating, CCK-8 solution was added to each well and measured at 450 nm using a microplate reader (Cytation5, Biotek). To determine the growth curve of PUMA KO HepG2 cells reconstituted with PUMA or PUMA mutants, cells were seeded onto 6-well plates (2000 cells/well) with media containing 0.5 μ g/ml Doxy to induce the gene expression. The number of cells in each well was counted every other day in triplicate.

Chemical and Cytokine Treatment

IKK β inhibitor IKK16 (Selleckchem) and TPCA-1 (Selleckchem) were dissolved in DMSO as a 10 mM stock solution. HepG2 cells were maintained in the resting state by culturing the cells in serum-free medium for 24 hours. The cells were treated with either TPCA-1 (5 μ M) or IKK16 (5 μ M) for 2 hr before being treated with 50 ng/ml TNF- α (Peprotech) for 2 hr. To activate p53 to levels that induce metabolic change but not apoptosis, HCC cells were treated with 0.3 μ M p53 activator RITA [(2,5-bis(5-hydroxymethyl)-2-thienyl) furan, Sigma] for 24 hr. Doxy stock solution (100 mg/ml) was purchased from Sigma. Due to the high instability of Doxy, Doxy-containing media were changed every day. ATPase inhibitor oligomycin was dissolved in DMSO or ethanol as a 10 mM stock solution. Cells were treated with 1 μ M oligomycin with or without 25 mM 2-deoxy-D-glucose (2-DG) (1M stock solution in PBS) (Sigma).

Mitochondria Isolation

Mitochondria were isolated from mouse tissues with Mitochondria Isolation Kit (Thermo scientific) according to manufacturer's instruction. Mouse liver tissues were washed twice with cold PBS, and 0.1 g tissue were homogenized in 800 μ l of BSA/Reagent A solution on ice using Dounce grinder (Sigma) (15–20 strokes). After adding 800 μ l of Mitochondria Isolation Reagent C, mixtures were centrifuged at $700 \times g$ for 10 min at 4°C. Supernatant was further centrifuged at 3000g for 15 min at 4°C. Mitochondria pellet was washed with 500 μ l of Wash buffer and maintained on ice for metabolic assays. Procedure for isolating mitochondria from culture cells was the same as above. In addition, sucrose-mannitol homogenizer buffer was used for mitochondria isolation. Sucrose-mannitol homogenizer buffer (70 mM sucrose, 250 mM mannitol, 0.1 K-EDTA mM, 0.5 mM K-EGTA, 10 HEPES pH 7.4) was freshly prepared from 5X buffer with Halt™ Protease & phosphatase inhibitors cocktail (Thermo). After the cells were washed with cold PBS twice and sucrose-mannitol homogenizer buffer once, cells were homogenized in 1X sucrose-mannitol homogenizer buffer with Dounce grinder on ice (15–20 strokes). After centrifugation at $600 \times g$ for 10 min at 4°C, supernatants were collected and further centrifuged at $8000 \times g$ for 10 min at 4°C.

Mitochondrial Pyruvate Uptake Assay

Mitochondria pellets were gently resuspended in 50 μ l cold respiration buffer (25 mM KCl, 20 mM HEPES, 4 mM MgCl₂, KH₂PO₄ pH7.4) and maintained on ice. Pyruvate uptake assay solution was prepared in lower pH respiration buffer (pH 6.8) with 0.4 mM pyruvate and 0.2 mM malate at room temperature. 10 μ l of resuspended mitochondria were added to 40 μ l of respiration buffer with MPC inhibitor UK5099 (Sigma) or DMSO. After adding pyruvate uptake assay solution, mixtures were incubated for 3 min at 37°C. To remove proteins and mitochondrial materials, 100 μ l 0.5 M monophosphoric acid (Cayman Pyruvate assay kit) was added into mixture, which was incubated for 3 min on ice and centrifuged for 3 min at 10000 rpm at 4°C. Supernatants were mixed with 5 M potassium carbonate (Pyruvate assay kit, Cayman) and centrifuged at 10000 rpm for 5 min at 4°C. Resultant supernatants were measured for pyruvate levels according to the manufacturer's protocol (Biovision). The amount of mitochondrial pyruvate uptake was determined by subtracting the amount of pyruvate remaining in the supernatant from the input amount of pyruvate. MPC-dependent mitochondrial pyruvate uptake was assessed by subtracting amount of pyruvate in mitochondria treated with MPC inhibitor (0.2 mM UK5099) from that without MPC inhibitor. Mitochondrial DNA (mtDNA) was determined by Quanti-iT PicoGreen kit (Thermo scientific) according to manufacturer's protocol and used for normalizing the number of mitochondria.

Measurement of ATP Levels

To measure the levels of glycolytic ATP production, 1×10^4 cells were seeded into each well of black 96 well plates. To normalize the levels of protein, the same number of cells were seeded into clear bottom 96 well plates. Cells were incubated in medium containing $1 \mu\text{M}$ oligomycin (Sigma) to inhibit mitochondrial oxidative ATP production or 25 mM 2-deoxy-D-glucose (2-DG) to inhibit glycolytic ATP production. After washing the cells with PBS, ATP levels were measured using ATPlite kit according to manufacturer's protocol (PerkinElmer). To investigate the effects of RITA on the glycolytic ATP production, HCC cells were incubated with $0.3 \mu\text{M}$ RITA for 24 hr and assayed for ATP levels. Total ATP production was calculated by subtracting the amount of ATP in cells treated with both oligomycin and 2-DG from the amount of ATP in cells without treatment. To normalize the number of cells, protein concentration was measured using Bicinchoninic Acid Protein Assay Kit (BCA, Sigma Aldrich) according to manufacturer's protocols.

To determine pyruvate driven mitochondrial ATP production, purified mitochondria were resuspended in luciferin-luciferase assay buffer containing pyruvate (5 mM pyruvate/ 5 mM malate) and 0.1 mM ADP as previously described. Briefly, freshly isolated mitochondria were resuspended in $50 \mu\text{l}$ of respiration buffer (pH 7.4) and maintained on ice. Mitochondria respiration solution was prepared in respiration buffer (pH7.4) with 10 mM pyruvate and 10 mM malate. After adding 1 mM ADP as stimuli to respire, luminescence was measured with microplate reader (NOVOstar or Cytation5). The negative control was mitochondria in luciferin-luciferase assay buffer with pyruvate but without ADP. The amount of ATP production was normalized by mtDNA or amount of mitochondrial protein.

After twelve human cancer cell lines with p53 inducible knockdown vector were incubated with or without $1 \mu\text{g/ml}$ of Doxy for 3 days, 1×10^4 cells were seeded into each well of black 96 well plates. The cells were washed with PBS twice and media changed with DMEM (Gibco) with 10 mM pyruvate, no glucose, and no glutamine for 8 hours. After being washed with PBS, ATP levels in the cells were measured according to manufacturer's protocol. To normalize the number of cells, protein concentration was measured using BCA Protein Assay Kit (Sigma Aldrich) as mentioned above.

Measurement of Lactate Levels

The levels of lactate were determined using lactate kit according to the manufacturer's protocol (Biovision). Briefly, cells were seeded at a density of 1×10^5 cells/well. Supernatant was collected the next day and immediately incubated with the same volume of 0.5 M MPA for 5 min on ice. After centrifugation at $10,000 \text{ rpm}$, supernatant was mixed with 0.25 M potassium carbonate and centrifuged at 10000 rpm for 5 min at 4°C . The supernatant was incubated with reaction mixtures for 20 min and measured with the microplate reader. Data were normalized by the number of cells.

FRET (Fluorescence Resonance Energy Transfer) Analysis

HEK 293T cells were transfected with plasmids expressing GFP- and/or mCherry-tagged proteins using Lipofectamine 2000 solution according to manufacturer's protocol. Transfected cells were plated onto glass bottom culture dishes (MatTek), which was coated with matrigel (Corning) and analyzed using a laser-scanning confocal microscope (Nikon A1R). GFP were excited at 488 nm and their signals collected in the eGFP filter (525nm) and Texas Red filter (595nm) by using $60\times$ oil objectives. Acceptor bleaching was performed with a Nikon A1 laser scanning confocal microscope with the FRET acceptor bleaching protocol. Pre-bleach and post-bleach images were taken as time-lapse series with the excitation of low intensity 488 nm laser and filters of $500\text{--}550 \text{ nm}$ for collecting GFP emission and $570\text{--}620 \text{ nm}$ for RFP emission. Acceptor bleaching was performed with a Nikon A1 laser scanning confocal microscope with the FRET acceptor bleaching protocol. The acceptor was bleached with high intensity 561 nm laser. For the FRET analysis of endogenous PUMA and MPC1, HepG2 cells were seeded onto glass bottom culture dishes (MatTek) coated with matrigel (Corning) and stained with primary antibodies, followed by incubation with cy5-conjugated anti-goat secondary antibody and cy3-conjugated anti-rabbit antibody for 1 hr at RT, mounted using Mowiol 4-88 (Electron Microscopy sciences) because Cy3-Cy5 pair can be easily photobleached. FRET analysis was performed using 561 nm and 647 nm laser. Acquired images were exported using NIS elements imaging software and analyzed using the AccPbFRET plugin (Roszik et al., 2008) for ImageJ. FRET efficiency was calculated in a defined ROI of FRET image in a manner of pixel by pixel.

Confocal Microscopy

1×10^4 HepG2 cells were seeded onto chamber slides coated with matrigel (Corning). After 16 hr, media were changed to FluoroBrite DMEM (Thermo) to reduce fluorescent background. After 24 hr, cells were washed twice with PBS and fixed with 4% paraformaldehyde (PFA) for 20 min at room temperature (RT). After washing with PBS three times, cells were permeabilized with 0.3% Triton X-100 in PBS for 10 min at RT, blocked with the blocking buffer (20% normal donkey serum, 3% BSA, 0.3% Triton X-100 in PBS) for 1 h at RT, then stained with anti-PUMA antibody (Novous, 1:40) and anti-MPC1 antibody (Novous, 1:20) at 4°C overnight, followed by simultaneous incubation with Alexa Fluor 568-conjugated anti-goat secondary antibody and Alexa Fluor 488-conjugated anti-rabbit antibody for 1 hr at RT. Slides were mounted using VECTASHIED solution (Vector) with DAPI. Confocal images were acquired at room temperature using $100\times$ high NA (1.49NA) oil objectives of the Nikon A1 system, equipped with Nikon Ti microscope, A1R hybrid confocal scanner of galvano and resonant, and LU4 four-laser AOTF unit with 405 , 488 , 561 , and 647 lasers and driven by NIS elements imaging software. For the colocalization analysis of PUMA and MPC, 405 , 488 , and 561 lasers were used to acquire images from which Person's correlation coefficients (PCC) and M1 Manders' correlation coefficients (MCC) were calculated within single cells using colocalization colormap plugin and Coloc2 plugin, respectively. While PCC is a useful statistic value to evaluate overall colocalization of PUMA and MPC1 in the acquired image, MCC is useful to evaluate the fraction of MPC1 that is closely colocalized

with PUMA. PCC value is ranged from 1 (the fluorescence intensities of PUMA and MPC1 are in perfect linear correlation) to -1 (the fluorescence intensities of PUMA and MPC1 are inversely correlated). MCC was calculated from the images exported by NIS elements imaging software using Coloc2 plugin.

Western Blotting and Co-immunoprecipitation

Cells were extracted for total proteins using lysis buffer (150 mM NaCl, 0.4 % Triton X-100, 0.2% NP-40, 10% glycerol 25 mM HEPES pH 7.4, Halt Protease and Phosphatase Inhibitor Cocktail). For mitochondrial fraction, purified mitochondria were incubated in the lysis buffer on ice for 30 min and centrifuged for protein extract. Samples were separated on 8-15% SDS PAGE and transferred to nitrocellulose membranes, which were blocked with blocking buffer (5% skim milk in PBS with 0.05 % Tween 20) and incubated with primary antibodies in the blocking buffer. After being washed three times with blocking buffer, the membrane was probed with a horseradish peroxidase-conjugated secondary antibody and developed with Supersignal West Pico or Dura (Thermo Fisher Scientific). For co-immunoprecipitation (Co-IP) of mitochondrial proteins, isolated mitochondria were applied to mitochondria immunoprecipitation kit (Sigma) according to manufacturer's instruction. Briefly, mitochondria were solubilized in mitochondria IP buffer with 0.6% n-Dodecyl β -D-maltoside and protease inhibitor cocktail on ice for 30 min. After the centrifugation at 12,000 \times *g* for 10 minutes at 4°C, supernatants were immunoprecipitated with antibodies followed by incubating with magnetic protein A/G beads (Pierce) for 2 hr at 4°C. For the pull-down of GFP tagged MPC1, cell lysates were applied to GFP-Trap according to the manufacturer's instruction (ChromoTek). For IP of phosphorylated PUMA, cells were collected in the IP lysis buffer (Thermo) with Halt Protease and Phosphatase Inhibitor Cocktail (Thermo). Cell lysates were immunoprecipitated with anti-phospho-serine antibodies (Abcam). The intensity of protein bands was quantified using ImageJ software (NIH). In case of using Chemidoc MP to detect signal from membrane, the intensity of protein bands was quantified using Image Lab (BioRad).

Flow Cytometry

To determine the levels of apoptosis induced by PUMA expression in PUMA KO cells, PUMA KO HepG2 cells reconstituted with PUMA or PUMA mutants were seeded onto 6-well plates (30,000 cells/ well) with media containing 0.5 μ g/ml Doxy to induce the expression. Cells were collected 24 hr later and stained with FITC-Annexin V and PI (Thermo scientific) according to manufacturer's protocol. Apoptotic cells were defined as double positive for PI and Annexin V.

Total RNA Extraction and cDNA Synthesis

RNeasy Mini Kit (Qiagen) was used to extract total RNA from cells according to the manufacturer's instructions. Cells were collected directly in the RLT lysis buffer. After brief pipetting in lysis buffer, cells were homogenized using QIAshredder (Qiagen) according to manufacturer's instructions and purified with RNeasy Mini kit columns. RNase-free DNase Kit (Qiagen) was applied to remove genomic DNA. TRIzol reagent (Thermo scientific) was used for RNA extraction from mouse liver tissues. 0.1 mg of liver tissues were homogenized in 1 ml TRIzol reagent with electric homogenizer and mixed with 0.2 ml chloroform vigorously (Sigma Aldrich). After incubating at room temperature for 3 min, the mixture was centrifuged at 10,000 for 15 min. Top aqueous phase containing RNA was collected, mixed with same volume of 100% ethanol, and loaded into RNeasy column. RNA concentration was determined by DU730 UV/Vis spectrophotometer (Beckman Coulter) at absorbance of 260 nm. cDNA synthesis from total RNA was performed using High Capacity cDNA Reverse Transcriptase Kit (Applied Biosystems) following the manufacturer's instructions. 1 μ g of total RNA was reversely transcribed with random hexamers. For cloning, cDNA was synthesized from 1 μ g of RNA extracted from hESC cells using SuperScriptIII Reverse Transcriptase Kit (Invitrogen).

Quantitative PCR Analysis

Real time PCR analysis was performed using StepOnePlus Real-Time PCR System (Applied Biosystems) with FastStart Universal SYBR Green Master (Roche) as previously reported (Kim et al., 2014). The PCR conditions were as follows: 10 min at 95°C, 40 cycles of 15 s at 95°C, and 1 min at 60°C. The average Ct value for each gene was determined from triplicate reactions and normalized with the amount of β -actin. Primer sequences are shown in Table S1.

Correlation Studies between PUMA Expression and Glycolysis of HCC Samples

Freshly resected HCC tissues were assayed for the levels of PUMA protein. The levels of lactate in HCC tissues were measured using PicoProbe Lactate assay kit (Biovision) according to the manufacturer's instructions. Pieces of tissues were homogenized in assay buffer with IKA ULTRA-TURRAX dispersers (IKA) and centrifuged to remove insoluble materials. The supernatant was immediately incubated with the same volume of 0.5 M MPA for 5 min on ice. After centrifugation at 10000 rpm, supernatant mixed in 0.25 M potassium carbonate was centrifuged at 10,000 rpm for 5 min at 4°C. Resultant supernatant was incubated with reaction mixture for 20 min and measured under the microplate reader (BioTek). To normalize results, protein concentration in homogenate without deproteinization procedure was determined by BCA assay. To measure cytoplasmic pyruvate, HCC tissues were minced and homogenized in bead homogenizer with homogenization buffer (220 mM mannitol, 70 mM sucrose, 5 mM HEPES-KOH pH 7.4, 1 mM EGTA-KOH pH 7.4., 1 ml per 0.1 g tissues). Homogenates were centrifuged at 600 \times *g* for 10 min at 4°C and supernatant further centrifuged at 8000 \times *g* for 10 min at 4°C. Resulting supernatant was used to measure pyruvate with the kit (Biovision). For mitochondrial pyruvate uptake assay, HCC tissues were minced and homogenized by Potter-Elvehjem PTFE glass homogenizer (Sigma Aldrich) with Sucrose-mannitol homogenizer buffer (70 mM sucrose, 250 mM mannitol, 0.1 K-EDTA mM, 0.5 mM K-EGTA,

10 mM HEPES pH 7.4., 1 ml per 0.1 g tissues; 25 strokes). Homogenates were centrifuged at $600 \times g$ for 10 min at 4°C and supernatant further centrifuged at $8000 \times g$ for 10 min at 4°C . Resulting mitochondrial pellets were re-suspended and incubated for 3 min at 37°C in 90 μl of respiration buffer (pH 6.8) with a mixture of 0.2 mM pyruvate and 0.1 mM malate with either 0.2 mM UK5099 (Sigma Aldrich), an inhibitor of mitochondrial pyruvate carrier (MPC) or solvent only control (DMSO). Amount of mitochondrial pyruvate uptake was determined by subtracting the amount of pyruvate remaining in the supernatant from initial amount of pyruvate. Mitochondrial DNA (mtDNA) was determined by Quanti-iT PicoGreen kit for normalization.

Survival Correlation Studies on Patient Samples

For the correlation studies of gene expression in HCC and survival of HCC patients, total RNA was extracted from previously frozen HCC tissues using TRIzol reagent (Thermo scientific) according to the manufacturer's instructions. cDNA was synthesized using PrimeScript cDNA kit (Takara Bio). Quantitative real-time PCR was performed with an SYBR Premix Ex Taq (Takara Bio). The primer sequences for 18S, p21, PUMA were provided in [Table S1](#). Sixty samples from the patients who died within 3 years after surgery were used for the survival correlation studies. Two of the 60 samples had no detectable p21 expression, and therefore, 58 samples were analyzed for the survival correlation studies of p21 expression. For sequencing p53 gene, total RNA was extracted from fresh HCC tissues using TRIzol reagent and cDNA was synthesized using PrimeScript cDNA kit. The region from exon 4 to exon 10 on p53 were amplified by PCR and sequenced. The postoperative survival rate was analyzed with the Kaplan-Meier method, and differences in survival rates were assessed with the log-rank test. Univariate and multivariate analyses were based on the Cox proportional hazards regression model. All the statistical analyses were performed with IBM SPSS Statistics 20.0 (IBM, IL, USA). Two-sided p values were calculated, and $p < 0.05$ indicates a statistically significant data.

Statistical Analysis

The statistical significance of Kaplan-Meier survival plot was determined by log-rank analysis. Univariate and multivariate analyses were based on the Cox proportional hazards regression model. Statistical significance on the comparison in tumor growth rates was tested by repeated measure ANOVA. To compare tumor weight between two groups, non-parametric Mann-Whitney test was used. Statistical significance between high-pyruvate-uptake HCC samples and low-pyruvate-uptake samples was tested by non-parametric Mann-Whitney test. Statistical significance of correlation between lactate and PUMA was tested by Pearson correlation test. For the rest of experiments, significant difference was determined by t-test and ANOVA. All the statistical analyses on patient's survival were performed with IBM SPSS Statistics 20.0 (IBM). Other analyses were performed in PRISM. The number of repeats was stated in the figure legend. No statistic method was used for determining sample size, blinding and randomizing.